Discover Applied Sciences

Research

Energetic analysis and economic viability of active atmospheric water generation technologies

Julius Potyka[1,2] · **Antoine Dalibard**[2] · **Günter Tovar**[1,2]

Received: 1 December 2023 / Accepted: 20 February 2024
Published online: 20 March 2024

Abstract
Water scarcity is a growing global and systematic problem in regions with low groundwater availability. Atmospheric water generation (AWG) technologies are an innovative solution to the water shortage problem, as atmospheric water vapor is a readily available resource even in arid regions, with the drawback of high energy consumption. In this paper, the viability of AWG technologies on an energy and economic level is investigated by thermodynamic modeling of three main active AWG systems consisting of cooling condensation, adsorption and absorption processes. A location analysis model is developed to evaluate the performance based on representative weather data of temperature, pressure and relative humidity over a period of one year to account for seasonal shifts and daily variations in climatic conditions. The specific energy consumption kWh/kg, water production trend and total specific cost are calculated for each technology. Water production by seawater desalination at the nearest coastline and transportation to the site by tanker truck, as well as bottled water prices, are used as benchmarks to assess economic viability. The results show that active AWG systems can only be an economically viable alternative if the water consumption site is relatively far from the coast or other water-rich regions and low electricity costs are available (distance >600 km, electricity price <0.10 US$/kWh). Compared to bottled water, all AWG technologies are in a competitive price range. Absorption systems have an energy efficiency advantage over conventional cooling condensation and adsorption systems (cooling condensation: average 0.42 kWh/kg; absorption: average 0.38 kWh/kg; adsorption: average 1.16 kWh/kg), but require a higher degree of process and plant design development. However, because of the high fluctuation in water production, atmospheric water generation technologies should be considered as a complementary supply to conventional water sources.

Article Highlights

- Modelling of three main atmospheric water generation systems using thermodynamic models to compare energy efficiency.
- Active atmospheric water generation systems can be energetically and economically feasible in beneficial circumstances.
- Due to the high fluctuation in water production, atmospheric water generation technologies should be seen as an additional supply to conventional water sources.

✉ Julius Potyka, julius.potyka@igvp.uni-stuttgart.de; Antoine Dalibard, antoine.dalibard@igb.fraunhofer.de; Günter Tovar, guenter.tovar@igvp.uni-stuttgart.de | [1]Institute of Interfacial Process Engineering and Plasma Technology (IGVP), University of Stuttgart, Pfaffenwaldring 31, 70569 Stuttgart, Germany. [2]Institute for Interfacial Engineering and Biotechnology (IGB), Fraunhofer, Nobelstraße 12, 70569 Stuttgart, Germany.

Keywords Atmospheric water generation · Atmospheric water harvesting · Absorption · Adsorption · Desorption · Condensation

1 Introduction

Securing the world's water supply is a major challenge for future generations [1, 2]. Freshwater scarcity is recognised as a global, systemic problem worldwide [3]. Already, two-thirds of the world's population experiences water scarcity for one month of the year, and half a billion people live in water-stressed areas throughout the year [4]. Total global water consumption increased by 13% from 3973 km^3/year in 2000 to 4489 km^3/year in 2021 [5]. During the same period, domestic water consumption increased by 33% from 384 km^3/year to 514 km^3/year, with a similar trend for future consumption [5, 6]. Due to population growth and rising average temperatures, water supplies are already severely constrained, especially in semi-arid and arid areas, as groundwater levels in many regions are being depleted faster than they can regenerate as a result of over-exploitation [7–9]. As a result, the transport and sale of water in tanker trucks or as bottled water is often the only supply option for people and industry in arid and non-coastal areas [10, 11]. In particular, the use of bottled water has increased dramatically in recent years, from about 200 million tons/year in 2010 to 355 million tons/year in 2021, with continued annual growth of 10% expected until 2026 [12]. The benefits of bottled water are consistent water quality, but high carbon emissions and plastic waste are important disadvantages [6, 12].

Seawater desalination, especially by reverse osmosis, is already a widely used water source in arid coastal regions such as the Arabian Gulf or the South American coast [13] , with more than 18,000 desalination plants in operation worldwide, producing about 40 billion m^3 of water per year [14, 15]. Its advantages are relatively low specific energy consumption of 3–5 kWh per m^3 of water produced [16, 17] and overall low production costs of 0.5−1.5 US$/$m^3$ [18–20], as well as large production capacities of up to 1 million m^3 per day [18, 20]. However, there are several environmental concerns, in particular the amount of chemicals used to pre-treat seawater and the large quantities of highly saline brine produced, which is discharged into the sea, endangering local coastal regions and marine life [21–23]. In addition, fossil fuels are often used to power desalination plants, resulting in a significant carbon footprint for the water produced of 2 kg_{CO_2}/m^3 [14, 17].

Atmospheric water generation (AWG) or atmospheric water harvesting is an emerging technology that has gained interest in recent years as an additional source of potable water in water stressed areas. Concepts are being explored in which AWGs can provide an additional source of water to increase the resilience of the overall water supply [24]. The global market for AWG systems is estimated at USD 2.1 billion for 2019 [25]. For the following years 2020 to 2027, market forecasts predict strong growth with an annual growth rate of 19.5% [25], which means that a global AWG market volume of around USD 10 billion can be expected by the end of the decade. AWG technologies can be divided into active and passive systems [3, 26]. Active systems allow greater scalability and more consistent water production from air, but require more energy and process engineering. Passive systems can operate independently of local infrastructural conditions such as power sources , etc., but are often very locally applicable (e.g. fog nets) or highly dependent on climatic conditions (e.g. solar radiation). Due to these disadvantages in scalability and high dependence on local conditions, only active AWGs are considered in this research article. Active AWGs can be divided into cooling and desiccant based systems. Cooling Condensation AWGs (CC AWGs) are an established technology and are widely available in the AWG market, where they account for 98.9% of global revenues [25]. However, CC AWGs have a limited application range in terms of climatic conditions due to the need to sub-cool the air below its dew point and high energy consumption ranging from 0.2−1.5 kWh/m^3 depending on climatic conditions [26, 27]. Desiccant based systems use either adsorption or absorption of atmospheric water. The adsorption process uses porous solid materials such as MOFs or zeolites to bind the water molecules and is the subject of much active research in terms of materials used and process application [28–31]. These adsorbents have highly variable water uptake potentials ranging from 0.2 to 1.6 $kg_{water}/kg_{desiccant}$ [30, 32], and optimization of the materials in terms of uptake potential and energy efficiency is a major area of current academic research. Energy requirements for adsorption–desorption AWG vary widely, ranging from 0.9–4 kWh/kg [26]. Absorptive processes use hygroscopic liquid salt solutions, for which various salts have been investigated for their process potential [33, 34], but the process engineering implementation of this technology has been sparsely explored [34] , with reported specific energy requirements of 0.15–1 kWh/kg [34].

The progress and comparison of different AWG technologies regarding their energy efficiency has been studied by several authors [3, 26, 35–38], which promises a possible implementation in the global water supply, although the high energy consumption is prominent in all active AWG technologies.

Lord et al. [39] explored the potential of cooling based AWGs for global application. Moghimi et al. [40] analyzed the profitability of a CC AWG machine in terms of its production and potential production and financial risks. However, in the current scientific literature, there is no comparison of the different active AWG technologies on a global scale in terms of performance evaluation (water production, energy efficiency) as well as economic comparison (water cost, production volatility). Furthermore, seasonal and intraday climatic variations have not been taken into account in the above mentioned research articles.

In this work, we present a modeling framework for a systematic comparison of the three defined active AWG technologies. These technologies are modeled and evaluated using hourly weather data over a representative year at 18 sites worldwide in terms of water production, energy consumption, water cost, and production volatility. From the results, considerations for the possible implementation of AWG technologies can be directly derived: On the one hand, the best choice of technology as well as the economic validity compared to conventional water sources such as seawater desalination or bottled water. Furthermore, the risk of fluctuating water production of the different technologies over the year is identified and the cost distribution of energy costs to investment costs in relation to the specific amount of water produced is compared in order to highlight possible optimization potentials with regard to the price of water.

2 Thermodynamic principles for water vapour extraction from air

The amount of water in the air is primarily affected by temperature, as warmer air has a greater capacity to hold moisture. The water content of air can be accurately measured by water vapour pressure, since the total pressure of gases is equal to the sum of their partial pressures. The saturation vapour pressure of air p_s corresponds to the liquid/gas phase boundary of water. Relative humidity ϕ_{rel} is expressed as the fraction of the actual vapour pressure over the saturation vapour pressure [41].

$$\phi_{rel} = \frac{P_v}{P_s} \tag{1}$$

The absolute amount of water in the air is given by the absolute humidity ϕ_{abs}, which measures the mass of water per volume of air. It is calculated from the vapour pressure, the specific gas constant R_v ($461.51\frac{J}{kg*K}$ for water) and the air temperature T in Kelvin [41].

$$\phi_{abs} = \frac{P_v}{R_v * T} \tag{2}$$

Changes in the moisture content of the air during extraction processes can be described energetically by the enthalpy of humid air.

$$h_{humidair} = c_{p,air} * T + x_{w,air} * (c_{p,wv} * T + \Delta h_v) \tag{3}$$

with the specific enthalpy $h_{humidair}$, the specific isobaric heat capacities of air and steam $c_{p,air}$ and $c_{p,wv}$, the mass fraction of water in the air $x_{w,air}$, the enthalpy of vaporisation Δh_v of water at 0 °C, and the air temperature T [41].

The density of humid air is calculated from the absolute humidity and the specific volume $v_{humidair}$ [41].

$$\rho_{humidair} = \frac{1 + \phi_{abs}}{v_{moistair}} \tag{4}$$

$$v_{humidair} = \frac{0.2871 * (T + 273.15) * (1 + 1.6078 * \phi_{abs})}{P} \tag{5}$$

The specific energy consumption (SEC) is used for the evaluation of thermal processes in terms of their energy efficiency [3, 26]. The SEC is calculated from the required energy input E per produced amount of water $\dot{m}_w$.

$$SEC = \frac{E}{\dot{m}_w} \tag{6}$$

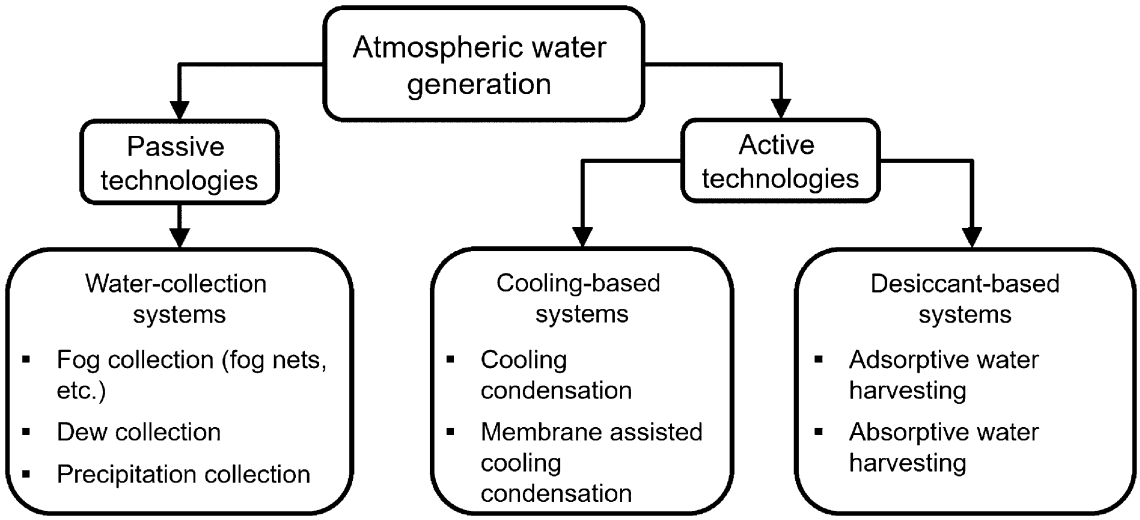

Fig. 1 Overview of AWG technologies, divided into in their respective categories

3 State of the art—air water generation technologies

Existing technologies for harvesting water from atmospheric moisture can be divided into passive and active systems [3], as shown in Fig. 1. Passive systems, such as fog or dew collectors, have the advantage of being simple to operate with low capital and maintenance costs, but are highly dependent on local climatic conditions [42]. Active systems, in contrast, are more scalable and less dependent on environmental conditions such as fog or sunlight [3]. Active technologies for extracting water from atmospheric moisture can be divided into two categories [34]: cooling-based systems and desiccant-based systems, which are further subdivided into adsorption-based processes using solid desiccants and absorption-based processes using liquid desiccants.

3.1 Passive air water generation technologies

Passive air water harvesting systems collect water from the air using natural processes without the need for external energy [3, 26]. These systems have the advantage of using simple technology, which means lower investment and operating costs. However, the low-tech nature of the systems also results in poorer adaptability to the environment . The yield is highly unpredictable due to weather and location dependency [3, 26, 42], as these systems are highly dependent on environmental conditions such as fog, dew or rain. Examples of passive air water harvesting systems are fog or dew nets, which collect the supersaturated water vapour in the air and allow it to condense on their surface, collecting the precipitating water [42]. These technologies are only suitable for use in regions with high humidity or precipitation, which are not typically regions affected by severe water scarcity, and are therefore not considered further in this study.

3.2 Active air water generation technologies

3.2.1 Active cooling condensation

Cooling condensation is the most widely used process to date for extracting water from atmospheric moisture [43] and is also commonly used in air conditioning systems to dehumidify the air. In this process, as shown schematically in Fig. 2, fans are used to bring air into contact with a cooled heat exchanger (condenser). In this condenser, the air is cooled below its dew point, condensating the atmospheric water in the air. The water is then discharged from the condenser and treated for the specific application. The yield of cooling condensation is highly dependent on relative humidity and air temperature and has limited application in cold dry areas where the dew point of the air is below the freezing point of water [27, 44]. Most refrigeration condensation processes are electrically powered. Cooling is provided by a vapour compression refrigeration cycle using refrigerants such as R-134a [45], where the electrical power requirement is determined by the energy efficiency ratio (EER) , which is defined as the ratio of the cooling energy supplied to the system

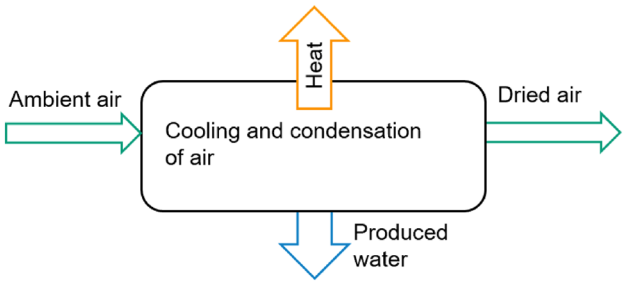

Fig. 2 Schematic of cooling condensation AWG. Ambient air is directed into cooling chamber by use of fan, in which it is then cooled below its dew point. The condensate is the generated product

to the electrical energy required as input [27]. The use of membranes to concentrate moisture in the incoming air can increase the efficiency and climatic range of application for the technology [46]. For reasons of simplicity in modelling the system, this addition is not considered in this study.

Typical machines available on the market, including their operating parameters as specified by the manufacturer, are listed in Table 1. An average of these parameters is used in the model to represent a representative machine.

3.2.2 Active adsorption–desorption using solid desiccants

Adsorption-based methods use a solid bed of microporous, hydrophilic material as the sorbent [28, 52]. Ambient air is passed through the adsorbent bed using a fan and the water molecules in the air are bound by physisorption in the hygroscopic pores of the adsorbent [52]. Unlike the cooling condensation method, the air does not have to be in a saturated state to collect the gaseous water, but it can be adsorbed directly from the air without the need for cooling. This process can be reversed by applying heat to the adsorbents. Novel metal-organic frameworks (MOFs) or special zeolite groups are commonly used as adsorbents [28–31]. Once maximum storage saturation is reached, the adsorbent is regenerated by heating the adsorbent bed. The produced water vapour is condensed in a condenser and the produced water can be treated. The process, as shown in the Fig. 3, must be cyclic when using a single adsorbent bed, e.g. a day-night cycle, where water is adsorbed at night and solar energy is used for desorption during the day [28]. Quasi-continuous operation can be achieved by using more than one adsorbent bed, which increases the complexity of the system. The commercialisation of this technology is still at the research stage, so there are no market-ready products.

3.2.3 Active absorption–desorption using liquid desiccants

Absorption-based systems use highly concentrated aqueous electrolyte solutions as liquid sorbents, which have hygroscopic properties. Similar to the adsorption process, no cooling or saturation of the air is required for the absorption to take place. The driving force for the mass transfer of the water between the gas and liquid phases is the difference between the vapour pressures of the gaseous and liquid water in each phase. When the vapour pressures are in equilibrium, no mass transfer takes place. This equilibrium describes the boundary between the absorption and desorption processes. Hygroscopic salts reduce the vapour pressure of the aqueous solution with increasing concentration, shifting the equilibrium in favour of absorption of water from the air into the liquid phase. The most commonly used salts for air dehumidification are lithium chloride (LiCl), magnesium chloride (MgCl2) or potassium acetate (KAC) [53–55]. Glycols such as triethylene glycol [54, 55] and ionic liquids [56, 57] are also used as hygroscopic sorbents. Compared to glycols, salts have the advantage that they have no vapour pressure and therefore remain in the aqueous phase when heated.

Table 1 Sample of large scale market availabe CC-AWG products including operating parameters as specified by producer

Brand	Max. water production [*L*/*day*]	Max. power supply [*kW*]	Air flow [m^3/h]	Price [*US$*]	References
GENAQ Technologies S.L.	5000	50	22,000	–	[47]
Watergen LTD	6000	60	–	90,000	[48]
AerOWater	1000	13	–	11,000	[49]
Aquaosmo	10,000	128	62,000	100,000	[50]
Imhotep Industries GmbH	10,000	120	–	–	[51]

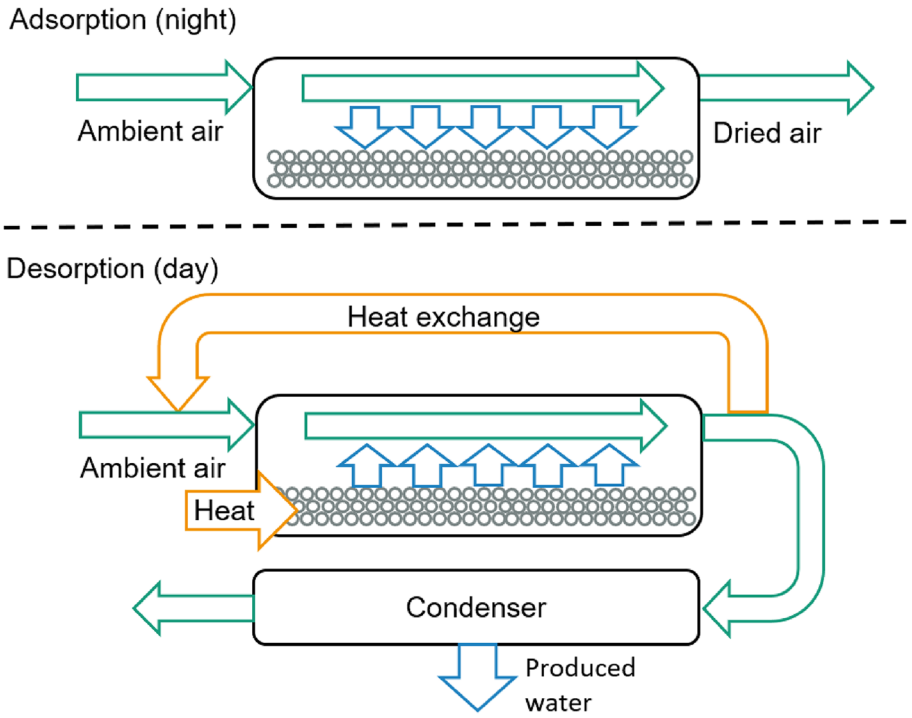

Fig. 3 Schematic of a two-stage adsorption–desorption process: In the adsorption stage (top), ambient air is brought into contact with the adsorbent, binding water to the adsorbent bed. In the desorption stage (bottom), the ambient air and the adsorbent bed are heated to desorption temperature, resulting in the evaporation of the bound water, which is then transported to the condensation chamber, where the humid air is cooled to condensation temperature

However, a disadvantage is that they typically have corrosive properties, which necessitates the use of more durable materials and results in higher investment costs [55]. Research into composite adsorbents using caged silica impregnated with lithium chloride or calcium chloride has shown that the corrosivity of these salts can be reduced while also improving the uptake kinetics [58, 59]. Further research in this area would help to drastically improve investment costs through the possible use of more cost effective material selection.

The schematic concept of an absorption–desorption system is shown in Fig. 4. The hygroscopic absorbent is brought into contact with the ambient air to allow the absorption of atmospheric water into the saline solution. In terms of process technology, the sorbent is either sprayed directly into the air to be dehumidified or distributed on the surface of solid structures, most commonly packed beds with loose packing [34]. The dilute electrolyte solution is then thermally heated so that the water can be evaporated, condensed and recovered. The concentrated electrolyte solution is recirculated to the absorption, allowing the process to be continuous [60]. Advantages over adsorption based processes are better scalability and continuous operation [60]. Compared to the cooling condensation process, higher energy efficiency and a wider climatic range

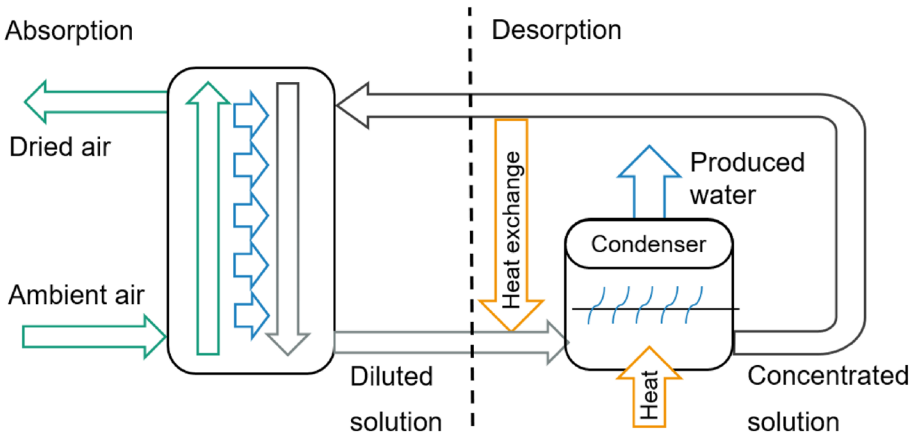

Fig. 4 Schematic of the absorption–desorption process using a liquid desiccant solution. In the absorption stage (left), liquid desiccant is brought into contact with the air by a fan and, depending on the ambient air conditions, binds water in the liquid phase. The diluted desiccant is then heated to evaporate the bound water, which is then condensed and collected in a condenser. The concentrated liquid desiccant is then pumped back to the absorption stage

are possible [3]. Similar to adsorption–desorption AWG, this technology is still at the research stage and no market-ready products are available.

3.2.4 Dessicant water uptake potential comparison

Figure 5 shows the water uptake potential of different desiccants per kg of adsorbent or per kg of absorbent solution at equilibrium at a fixed temperature of 15 °C (left) and 30 °C (right). At higher temperatures and humidity levels, a much higher sorption capacity can be achieved with liquid sorbents than with solid sorbents. However, in drier and colder conditions, the solid sorbents have a higher sorption capacity. Liquid sorbents are more sensitive to temperature than solid sorbents in terms of uptake potential. Comparatively, lithium chloride solution has a higher uptake potential than potassium acetate solution, but has significant other downsides such as high corrosiveness and toxicity, requiring more corrosion resistant materials and higher safety standards. For solid desiccants, the metal-organic framework MIL-101(Cr) has the highest absorption potential at higher relative humidities. At lower relative humidities, various solid desiccants such as MIL-160 have a higher water absorption potential. The complete adsorption–desorption cycle is illustrated in Fig. 20, showing the shift of the adsorption isotherm for the higher desorption temperature at 70 °C.

4 Modelling of active AWG technologies and location analysis

4.1 Cooling condensation model

Cooling condensation works by lowering the ambient air temperature below its dew point. The model consists of mass and energy balances of this process to calculate the outlet air temperature and the specific energy consumption, as shown in Fig. 6. Table 2 lists the required input data for the cooling condensation AWG (CC AWG) model; Table 3 lists the model parameters with their chosen values.

The power required for the fan is given by the pressure drop in the CC AWG δp and the inlet airflow.

$$E_{elec.,fan} = \frac{\delta p * \dot{V}_{air,in}}{\eta_{fan}} \tag{7}$$

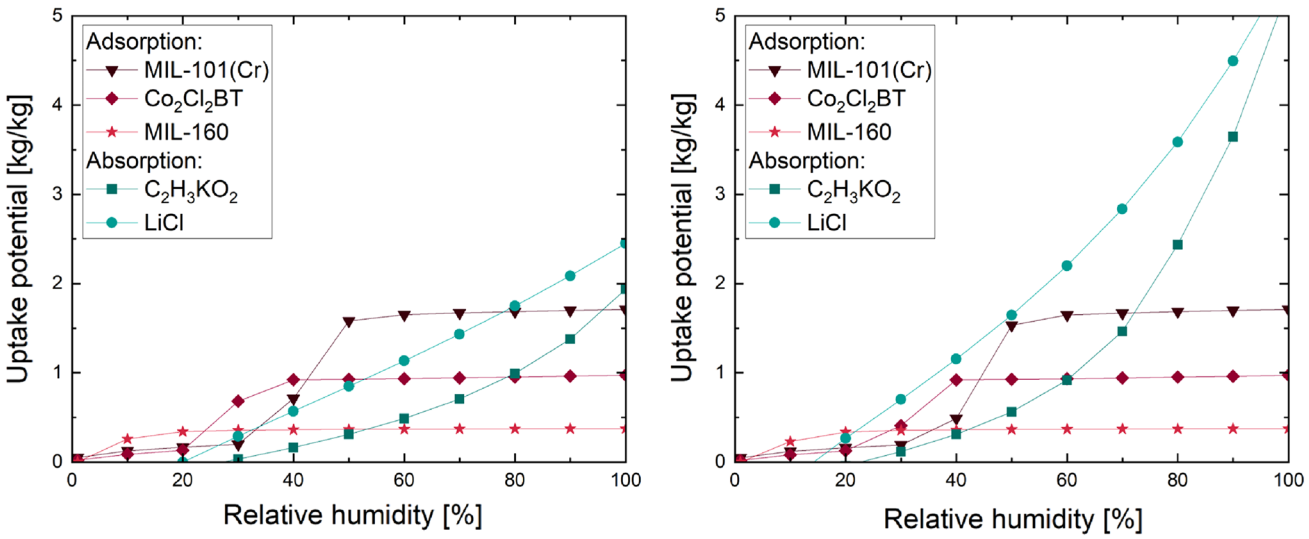

Fig. 5 Water uptake potential in kilograms of water per mass of sorbent at a temperature of 15 °C (left) and 30 °C (right). Adsorbent material data from Gordeeva et al. [61]. Vapour pressure data for lithium chloride uptake potential near the solubility limit (45 weight %) from Chaudhari and Patil [62]. Correlations based on vapour pressure measurements from Kölking [34] are used to calculate the uptake potential of potassium acetate near the solubility limit (75 weight %)

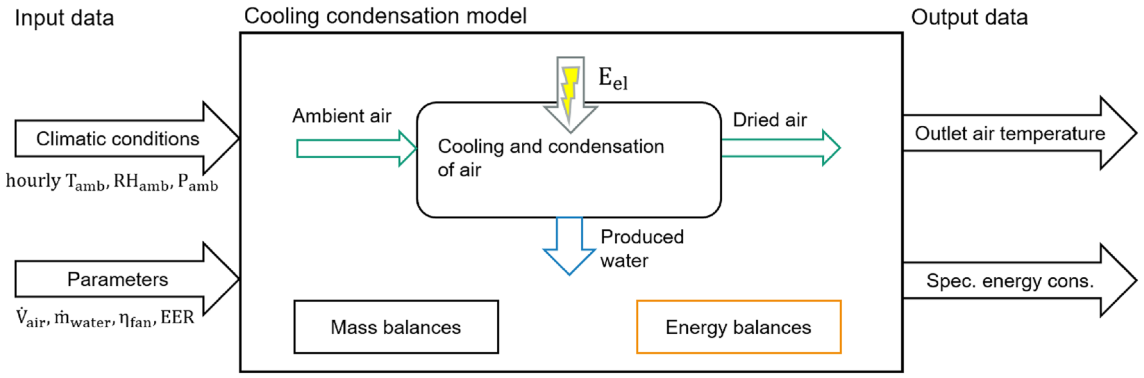

Fig. 6 Schematic of the cooling condensation AWG model with input and output data

Table 2 Required input data for the cooling condensation AWG model

Input data	Unit
Hourly temperature	[°C]
Hourly relative humidity	[%]
Hourly ambient pressure	[mbar]

Table 3 Model parameters with their chosen values for the cooling condensation AWG model

Model parameter	Value	Unit	References
EER	5	[–]	[27, 46]
Pressure loss δp	2	[mbar]	Assumed
E_{el}	50	[kW]	See Table 1
$\dot{V}_{air,in}$	22,500	[m^3/ h]	See Table 1
Efficiency fan η_{fan}	0.5	[–]	Assumed
Overall heat loss coefficient k_{loss}	10	[W/m^2K]	[63]
Surface area of heat loss A_{loss}	35	[m^2]	See Table 1

The absolute humidity, enthalpy and density of the inlet air are calculated according to the thermodynamic principles of water vapour extraction from air as described in Sect. 2. The inlet air mass flow rate is calculated from the inlet air volumetric flow rate and the air density.

$$\dot{m}_{air,in} = \rho_{air,in} * \dot{V}_{air,in} \tag{8}$$

The dry air mass flow rate at the inlet and outlet of the AWG is constant, as only water is condensed during the process.

$$\dot{m}_{dryair} = \frac{\dot{m}_{air,in}}{\phi_{air,in} + 1} \tag{9}$$

The total mass balance and the water mass balance are used to calculate the exhaust air mass flow and the exhaust air absolute humidity and temperature.

$$\dot{m}_{air,out} = \dot{m}_{dryair} * (\phi_{air,out} + 1) \tag{10}$$

$$\phi_{air,out} = \frac{\dot{m}_{air,in} * \phi_{air,in} - \dot{m}_{water}}{\dot{m}_{air,in} - \dot{m}_{water}} \tag{11}$$

The enthalpy of the outgoing air stream is calculated from the temperature and absolute humidity. The cooling energy required is calculated from the total energy balance.

$$\dot{Q}_{cool} = \dot{m}_{air,in} * h_{air,in} - \dot{m}_{air,out} * h_{air,out} - \dot{m}_{water} * h_{water} - \dot{Q}_{loss} \tag{12}$$

$$\dot{Q}_{loss} = k_{loss} * A_{loss} * (T_{air,out} - Tair, in) \tag{13}$$

The electrical energy input can be expressed using the EER and the required cooling energy as

$$E_{elec.,cool} = \frac{\dot{Q}_{cool}}{EER}. \tag{14}$$

The total specific energy consumption of the CC AWG is given by

$$SEC = \frac{E_{elec.,cool} + E_{elec.,fan}}{\dot{m}_w}. \tag{15}$$

4.2 Adsorption–desorption model

The model is divided into two parts, one being the adsorption of humidity during the night and the other being the desorption and condensation of water during the day, as shown in Fig. 7. The reasonable assumption is that the adsorption and desorption kinetics are fast enough to allow for a day-night cycle [52]. The assumed cycle lengths are 12 h each (desorption 8 am–8 pm, adsorption 8pm-8am). Climatic data averaged over the cycles are then used as input to the model. Assumptions made for modelling the absorption–desorption system:

- Adsorption and desorption kinetics are fast enough to be completed in a 12 h cycle [26, 30].
- Uniform airflow through the adsorbent bed.
- Uniform heating of the adsorbent bed.
- Ambient temperature is used as condensation temperature in the desorption stage.

Table 4 lists the required input data for the adsorption–desorption AWG model. Table 5 lists the model parameters with their selected values.

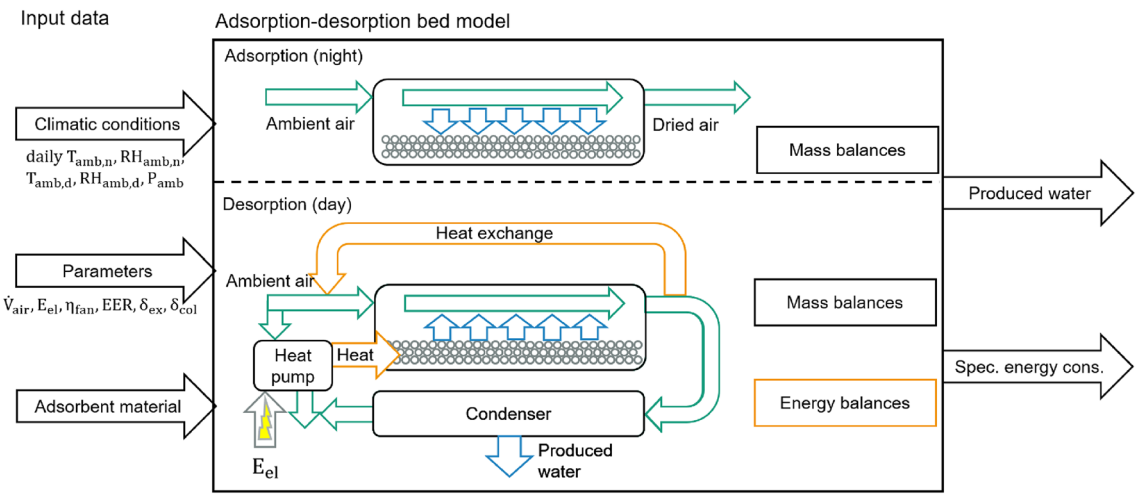

Fig. 7 Schematic of the adsorption–desorption AWG model with input and output data

Table 4 Required input data for the adsorption–desorption AWG model

Input data	Unit
Daily average day temperature	[°C]
Daily average day temperature	[°C]
Daily average day relative humidity	[%]
Daily average day relative humidity	[%]
Average yearly ambient pressure	[mbar]

Table 5 Modell parameters with their chosen values for the adsorption–desorption AWG model

Model parameter	Value	Unit	References
COP	5	[–]	[64]
Pressure loss in adsorption bed δp	2	[mbar]	Assumed
Mass of adsorbent material	1000	[kg]	Assumed
Air flow in unit $\dot{V}_{air,ad}$	10,000	[m^3/h]	Assumed
Efficiency fan η_{fan}	0.5	[–]	Assumed
Overall heat loss coefficient k_{loss}	10	[W/m^2K]	[63]
Surface area of heat loss A_{loss}	35	[m^2]	Assumed
Water collection fraction δ_{col}	0.7	[–]	[61]
Adsorbent material properties			
Adsorption enthalpy		[kJ/kg]	[32, 61]
Uptake capacity parameters		[–]	[32, 61]
Adsorbent heat capacity		[kJ/kg]	[31, 32, 61]
Binder material heat capacity		[kJ/kg]	[32, 61]

To simplify the model, the reasonable assumption of the Polanyi principle of temperature invariance for the water adsorption equilibrium is used [61]. Thus, the Polanyi adsorption potential ΔF_{ad} is given by

$$\Delta F_{ad} = -R * T * ln\left(\frac{P_v}{P_s(T)}\right) \tag{16}$$

using the ambient vapour pressure P_v and the saturation vapour pressure $P_s(T)$ at the ambient temperature T. The amount of water adsorbed per mass of adsorbent is then calculated as follows [61].

$$w_{ad} = \frac{A * (\Delta F_{ad}/1000) + B}{1 + exp(-k_1 * (\Delta F_{ad}/1000) - x_1)} + \frac{C}{1 + exp(-k_2 * (\Delta F_{ad}/1000) - x_2)} \tag{17}$$

where A, B, k_1, x_1, k_2 and x_2 are adsorbent material parameters as described by Gordeeva et al. [61] for different bed materials.

The desorption temperature depends on the adsorbent material and the target water collection fraction, which describes the fraction of water collected during the desorption phase and can be calculated from the saturation pressure of water and the outlet vapour pressure at the desorption temperature [61].

$$\delta_{col} = 1 - \frac{P_v(T_{day})}{P_{out,des}(T_{des})} \tag{18}$$

The water collection fraction is set to a reasonable value of 0.7 [61]. The desorption potential ΔF_{des} is calculated using the desorption temperature, similar to the adsorption potential. The amount of water harvested per cycle is then given by

$$\Delta w_{cycle} = w_{ads} - w_{des} \tag{19}$$

The total amount of water produced per cycle depends on the amount of adsorbent used.

$$m_{w,cycle} = \Delta w_{cycle} * m_{adsorbent} \tag{20}$$

The total amount of air required for the desorption cycle also depends on the absolute humidity before (a) and after (b) the condensation step.

$$m_{air,cycle} = \frac{m_{w,cycle}}{\phi_{abs,a} - \phi_{abs,b}} \tag{21}$$

The desorption cycle time is calculated with Eq. (22).

$$\Delta t_{cycle} = \frac{m_{air,cycle}}{\dot{V}_{air,ad} * \rho_{air}} \tag{22}$$

Using the heat capacities of the adsorbent and binder materials, the required amounts of heating of the adsorbent bed and air as well as the adsorption energy and the energy losses to the environment can be calculated as [32]

$$Q_{tot,des} = Q_{heat,ad,bed} + Q_{heat,air} + Q_{adsorption} + Q_{loss}. \tag{23}$$

$$Q_{heat,ad,bed} = \left(\frac{c_{p,adsorbent} + c_{p,binder}}{\Delta w_{cycle}} + c_{p,w}\right) * (T_{des} - T_{day}) * m_{w,cycle} \tag{24}$$

$$Q_{heat,air} = m_{air,cycle} * (h_{air,a} - h_{air,b}) \tag{25}$$

$$Q_{adsorption} = m_{w,cycle} * h_{ads} \tag{26}$$

$$Q_{loss} = k_{loss} * A_{loss} * (T_{des} - T_{day}) * \Delta t_{cycle}. \tag{27}$$

The electrical demand for the heating is assumed to be supplied by a heat pump system, whose energy performance is defined by the coefficient of performance (COP), which describes the ratio of the electrical energy to the thermal energy supplied to the system. The COP value depends on the temperature rise required by the heat pump system. A value of 5 is chosen for the lower desorption temperatures of the adsorption–desorption AWG [64].

$$E_{elec,des,cycle} = \frac{Q_{tot,des}}{COP} \tag{28}$$

The power requirement for the fan is calculated as

$$E_{elec,fan,cycle} = \frac{\delta p * V_{air,cycle}}{\eta_{fan}}. \tag{29}$$

With the different energy consumption, the total specific energy requirement of the adsorption–desorption AWG model is calculated as follows.

$$SEC = \frac{E_{elec,des,cycle} + E_{elec,fan,cycle}}{m_{w,cycle}}. \tag{30}$$

4.3 Absorption–desorption model

The absorption–desorption model consists of two stages, an absorption stage and a desorption stage, see Fig. 8. In the absorption unit, a loose packing column with a high enough packing height is used so that the contact time between the air and the salt solution is long enough for equilibrium between the two phases to be reached [34, 60]. The diluted brine is then heated to its boiling point and the outlet concentration is set to a fixed value chosen to be close to the solubility limit. Assumptions made for modelling of the absorption–desorption system:

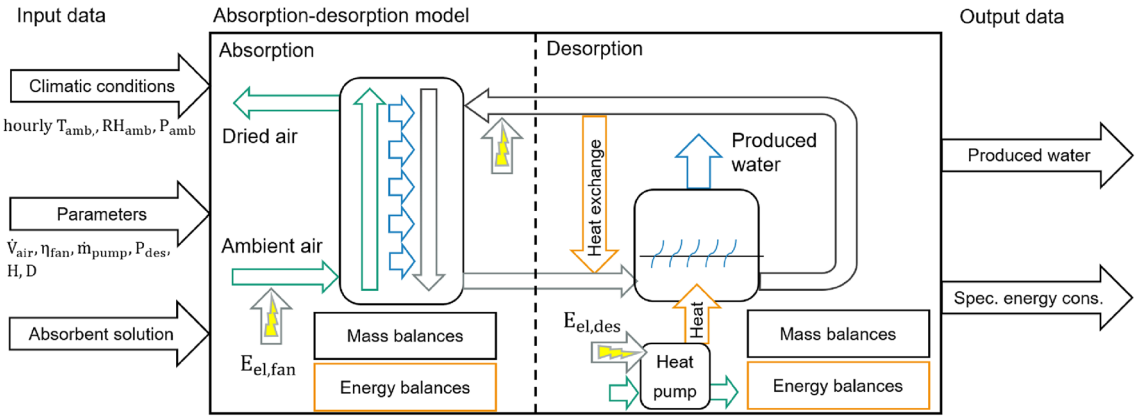

Fig. 8 Schematic of the absorption–desorption AWG model with input and output data

- The height of the absorption column is long enough to absorb atmospheric water up to the equilibrium state of air and salt solution [34, 60].
- The salt solution has the same temperature as the ambient air at the solution outlet of the absorption stage due to the high flow rate of air compared to the flow rate of salt solution and the large contact area.

Table 6 lists the required input data for the absorption–desorption AWG model. Table 7 lists the model parameters with their selected values.

In the absorption phase of the model, the equilibrium state of the solution and the corresponding humidity are calculated from the vapour pressure data (see Sect. 3.2.3). If no absorption is possible, i.e. the operating point would be on the desorption side of equilibrium and there would be mass transfer of water from the brine to the air, all variables are set to zero. The mass concentration of the saline solution after the absorption unit is calculated as

Table 6 Required input data for the absorption–desorption AWG model

Input data	Unit
Hourly temperature	[°C]
Hourly relative humidity	[%]
Hourly ambient pressure	[mbar]

Table 7 Modell parameters with their chosen values for the absorption–desorption AWG model

Model parameter	Value	Unit	References
COP	3	[–]	[64]
Pressure loss in column δp	3	[mbar]	Assumed
Mass flow of salt solution $\dot{m}_{sol,ab}$	3.5	[kg/s]	[60]
Air flow in unit $\dot{V}_{air,ab}$	22,500	[m^3/h]	[60]
Efficiency fan η_{fan}	0.5	[–]	Assumed
Efficiency pump η_{pump}	0.8	[–]	Assumed
Overall heat loss coefficient k_{loss}	10	[W/m^2K]	[63]
Surface area of heat loss A_{loss}	35	[m^2]	Assumed
Pumping height of overall unit H	5	[m]	Assumed
Pressure in desorption unit p_{des}	1000	[mbar]	Assumed
Heat exchanger temperature difference ΔT_{hx}	15	[K]	Assumed
Absorbent material properties (LiCl and KAC)			
Equilibrium curve of absorbent/air	f(T,x,P)	[mol/mol]	[34, 62]
Solubility limit of absorbent in water/inlet mass concentration		[kg/kg]	[34, 62]
Saturation pressure of absorbent	f(T,x)	[mbar]	[34, 62]

$$w_{ab,out} = \frac{\dot{m}_{sol,ab,in} * w_{ab,in}}{\dot{m}_{sol,ab,in} + \dot{m}_{air} * (y_{air,in} - y_{air,out})} \tag{31}$$

where $\dot{m}_{air}$ is the air mass flow rate, $\dot{m}_{sol,ab,in}$ the solution inlet flow rate, $w_{ab,in}$ the solution inlet salt mass fraction, $w_{ab,out}$ the solution outlet salt mass fraction, $y_{air,in}$ the air inlet water mass fraction and $y_{air,out}$ the air outlet water mass fraction. The air inlet mass flow rate is calculated from the air volume flow rate.

$$\dot{m}_{air,in} = \rho_{air,in} * \dot{V}_{air,in} \tag{32}$$

$$E_{elec,fan} = \frac{\delta p * \dot{V}_{air,in}}{\eta_{fan}} \tag{33}$$

The mass flow rate of the brine leaving the absorption unit is calculated from the total mass balance

$$\dot{m}_{sol,ab,out} = \dot{m}_{sol,ab,in} * \frac{w_{ab,in}}{w_{ab,out}} \tag{34}$$

with

$$\dot{m}_{sol,ab,out} = \dot{m}_{sol,des,in} \tag{35}$$

and

$$w_{ab,out} = w_{des,in}. \tag{36}$$

The required temperature in the evaporation unit and the outlet concentration of the absorption unit is calculated from the vapour pressure data of the absorption solution (physical property data of lithium chloride solution as described by Chaudhari and Patil [62], physical property data of potassium acetate from measurements of vapour pressure and heat capacity as described by Kölking [34]).

$$T_{des} = f(w_{ab,out}, p_{des}) \tag{37}$$

$$w_{ab,out} = f(T, RH, w_{ab,in}) \tag{38}$$

The amount of water evaporated is calculated from the total mass balance of the desorption unit.

$$\dot{m}_{des,w} = \dot{m}_{sol,des,in} - \dot{m}_{sol,des,out} \tag{39}$$

$$\dot{m}_{sol,des,out} = \dot{m}_{sol,des,in} * \frac{w_{des,in}}{w_{ab,in}} \tag{40}$$

The energy balance of the desorption unit is used to calculate the required heating energy $\dot{Q}_{des}$, which is provided by a heat pump with a fixed COP set to a value of 3, since the temperature rise is higher compared to the adsorption–desorption AWG [64]. The salt solution enthalpies are calculated using aforementioned physical property data [34, 62].

$$\dot{Q}_{des} = \dot{m}_{des,w} * h_{w,des} + \dot{m}_{sol,des,out} * h_{sol,des,out} - \dot{m}_{sol,des,in} * h_{sol,des,in} + \dot{Q}_{loss} \tag{41}$$

$$h_{sol} = f(T, w) \tag{42}$$

$$\dot{Q}_{loss} = k_{loss} * A_{loss} * (T_{des} - Tair) \tag{43}$$

$$E_{elec,des} = \frac{\dot{Q}_{des}}{COP} \tag{44}$$

The inlet temperature to the evaporator after heat exchange of the desorption outlet solution flow and the inlet solution flow is calculated using a simple heat exchanger calculation.

$$T_{des,in} = T + \frac{\dot{m}_{sol,des,out}}{\dot{m}_{sol,des,in}} * (T_{des} - T - \Delta T_{hx}) \tag{45}$$

where ΔT_{hx} is the temperature difference between the heat exchanger inlet and outlet flows. Using the hydrostatic pressure p_{hyd} and the hydraulic work W_{hyd}, the eletrical power consumption for pumping is calculated as

$$E_{elec,pump} = \frac{W_{hyd}}{\eta_{pump}} \tag{46}$$

with

$$W_{hyd} = \frac{\dot{m}_{sol,ab,in}}{\rho_{sol}} * p_{hyd} \tag{47}$$

and

$$p_{hyd} = \rho_{sol} * g * H. \tag{48}$$

The total specific energy consumption of the absorption–desorption AWG is then given by

$$SEC = \frac{E_{elec,des} + E_{elec,fan} + E_{elec,pump}}{\dot{m}_{des,w}}. \tag{49}$$

4.4 Reverse osmosis water production and transport model

The cost of producing water by reverse osmosis (RO) plant depends on the annual/daily water production capacity. With increasing capacity, the specific production cost decreases to a lower limit of about 0.50 \$/m^3 at 320,000 m^3/day. The specific cost is higher at lower production capacities, increasing significantly to about 2 \$/m^3 at 3000 m^3/day, with a maximum of 10–12 \$/m^3 at very low production capacities of around 100 m^3/day [18, 65, 66]. A fitted function of RO plant specific production costs in \$/m^3 as a function of daily water production in m^3, regressed from data in Al-Karaghouli and Kazmerski [18], Caldera et al. [19] and Ghaffour et al. [20]:

$$Cost_{RO} = 2.4858 * WP_{daily}^{-0.099} \tag{50}$$

The cost of transporting the produced water from the onshore RO plant to the site is calculated using a water tanker transport model [18, 67–70]. Tanker truck specific cost $Cost_{transport,truck}$ is calculated using the model developed by Marufuzzaman et al. [67] and Berwick as well as Farooq [68] and Pootakham et al. [69, 70] using the physical properties of water. Figure 9 shows the schematic of the RO and transport model. Table 8 lists the parameters required for the cost estimation model of water transport by truck.

The total cost of the produced and transported water is as follows.

$$Cost_{RO+transport} = Cost_{RO} + Cost_{transport,truck} \tag{51}$$

4.5 Overall location analysis and economic analysis model

All models are implemented in Matlab. Representative annual hourly weather data (temperature, relative humidity, air pressure) are generated for each site using Meteonorm 8.0 [71]. The location data and climatic conditions are used as an input to the model. With the calculated SEC over the whole year, the specific electricity cost per produced amount of water is calculate as

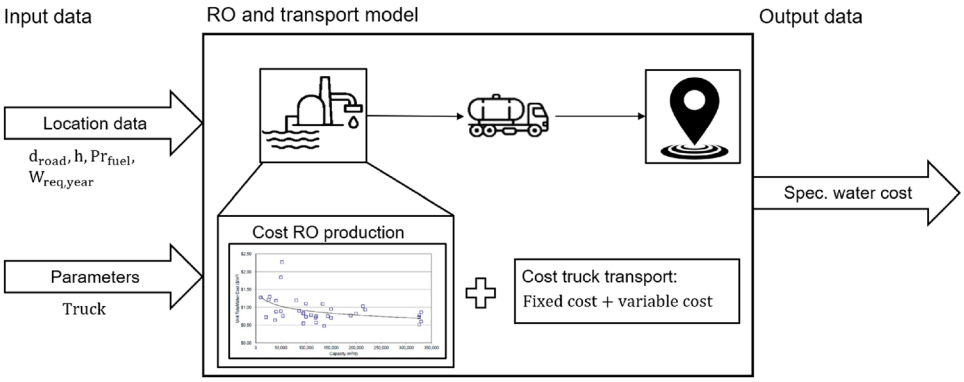

Fig. 9 Schematic of model for calculation of specific water cost via RO production and transport via truck

Table 8 Parameters required for water truck transport cost model and their chosen values [18, 67–69]

Parameter	Value	Unit	Comment/ References
Truck purchase price	80,000	[$]	[67]
Salvage value	30	[% of purchase price]	[68]
Interest rate	8	[%]	Assumed
Estimated useful lifetime of truck	5	[years]	[67]
Average transport speed	50	[km/h]	Assumed
Time loaded	50	[% of total time]	Assumed
Time empty	50	[% of total time]	Assumed
Fuel used in operation of trucks	Diesel	[–]	Assumed
Fuel efficiency loaded	46	[L/100 km]	[68]
Fuel efficiency empty	35	[L/100 km]	[68]
Labour rate per hour	10	[$/h]	[67]
Labour rate per km	0.21	[$/km]	[67]
Gross vehicle weight loaded	35,000	[kg]	Assumed
Gross vehicle weight empty	20,000	[kg]	Assumed
Truck capacity	15	[m^3]	Assumed
Base repair and maintenance cost	0.12	[$/km]	[67]
Tire cost	480	[$/tire]	[67]
Life of tire	430	[km]	[67]
Number of tires per truck	12	[–]	Assumed

$$Cost^{el}_{water,spec} = SEC * Cost_{elec}. \quad (52)$$

The three different AWG technologies are compared from an energy and economic point of view using the benchmark technology of RO water production and truck transport to the point of use. Figure 10 shows the schematic of the overall model with input and output data with the four sub-models.

To assess the potential for atmospheric water production, characteristic locations around the world are selected with a variety of different climatic conditions, distances from the coast, and different energy and fuel costs. Different economic and environmental zones, climatic conditions and levels of drinking water scarcity have been considered on all continents to provide a representative assessment, as listed in Table 9. Electricity and fuel costs were researched for a fixed date in 8/2023 [72]. The road distance to the site from the nearest coast was estimated using Google Maps [73]. Representative hourly climate data (temperature, relative humidity, pressure) were generated using Meteonorm 8.0 software [71].

The economic performance of the AWG technologies is assessed by calculating the total specific cost of produced water and a risk assessment of the volatility of production over the course of a year. The total specific water cost $Cost_{water,tot}$ is the sum of the specific electricity cost $Cost^{el}_{water}$ and the fixed annual cost $FC_{AWG,year}$ divided by the annual water demand W_{year}.

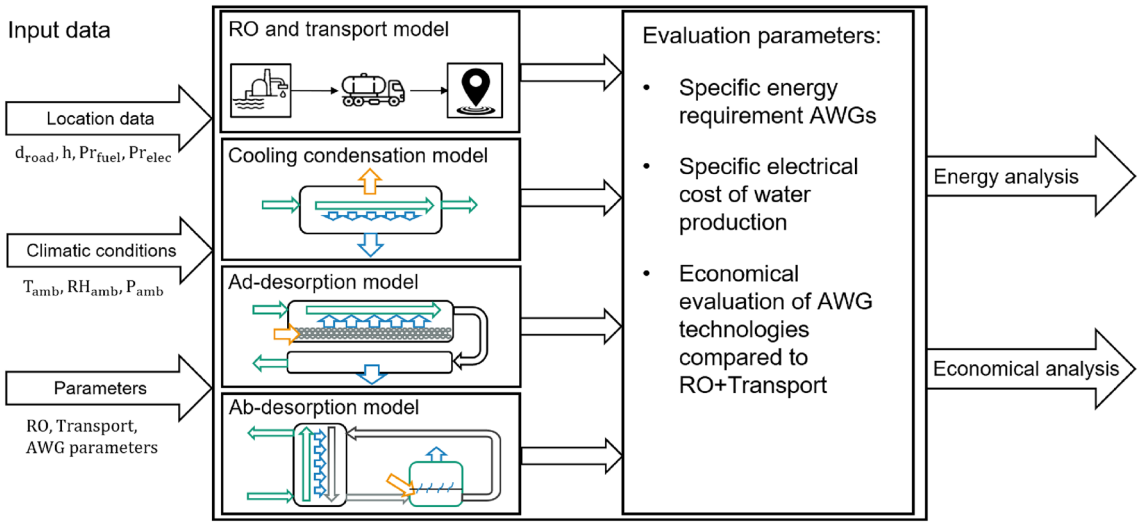

Fig. 10 Overall model approach for evaluation of active AWG technologies in different locations and climatic conditions

Table 9 List of sites selected for analysis with their relevant parameters of distance from shore, fuel and energy costs, average absolute humidity over a year and local bottled water cost [71–74]

Country	City	Distance road [km]	Electricity cost [$/kWh]	Fuel cost diesel [$/L]	Average absolute humidity [g_w/kg_{air}]	Bottled water cost [$/L]
S. Africa	Bloemfontein	600	0.074	1.28	5.64	0.63
S. Africa	Cape Town	–	0.074	1.28	8.61	0.63
Sudan	Khartoum	770	0.02	1.04	7.64	0.67
Senegal	Dakar	–	0.17	1.25	15.12	0.67
Morocco	Marrakesh	150	0.11	1.25	7.54	0.33
India	Solapur	430	0.08	1.13	12.31	0.24
India	Nagpur	780	0.08	1.13	12.66	0.24
U.A.E	Dubai	–	0.08	0.83	12.68	0.47
Qatar	Doha	–	0.02	0.56	12.78	0.23
Turkey	Ankara	270	0.09	1.10	5.41	0.53
Australia	Canberra	150	0.23	1.20	6.49	1.30
Spain	Madrid	400	0.24	1.66	5.81	0.53
USA	Los Angeles	–	0.15	1.08	8.76	0.97
USA	Denver	1600	0.15	1.08	4.27	0.97
Mexico	Mexico City	300	0.10	1.30	6.49	0.49
Chile	Santiago	100	0.13	1.35	6.64	0.63
Ecuador	Quito	270	0.09	0.46	7.59	0.59
Peru	Lima	–	0.16	1.26	13.67	0.33

$$Cost_{water,tot} = Cost^{el}_{water} + \frac{FC_{AWG,year}}{W_{year}} \tag{53}$$

The fixed costs include the annual price of the AWG, $P_{AWG,annual}$, and the maintenance costs, $Cost_{maint,annual}$, as a percentage of the investment costs. It is set at 3% of the annual investment cost for all AWG technologies [75].

$$FC_{AWG,year} = P_{AWG,annual} * (1 + C_{maint,annual}) \tag{54}$$

The annual depreciation is calculated using the total cost per AWG unit P_{AWG}, the total number of AWG units $n_{AWG,req}$ required to produce the specified amount of water, and the operating life of the AWG unit OL_{AWG}. The operating life of all AWG technologies is set to 15 years with no salvage value at the end.

$$P_{AWG,annual} = P_{AWG} * \frac{n_{AWG,req}}{OL_{AWG}} \tag{55}$$

$$n_{AWG,req} = \frac{W_{year}}{m_{water,total,year}} \tag{56}$$

The ratio of energy cost to total water cost is calculated to evaluate the impact of optimising energy consumption versus production cost savings. A higher value indicates a greater impact of energy costs on total water costs. It can therefore be concluded that either optimising energy consumption or reducing production costs will have a greater impact on the resulting total water costs and should be pursued with higher priority.

$$Eval_{elec/total} = \frac{Cost^{el}_{water}}{Cost_{water,tot}} \tag{57}$$

Table 10 lists the parameters chosen for the economic calculations. The purchase price for the CC AWG is chosen as an average of the values in Table 1. For the adsorption–desorption AWG and the absorption–desorption AWG there are no products on the market yet, therefore the purchase prices have to be estimated and are assumed to be twice as high as for the CC AWG due to the higher complexity of the technologies involved.

The volatility of AWG water production due to seasonal climatic variations poses a risk to the availability and reliability of water supplies. This is considered to be one of the major barriers to the adoption of AWG technologies [40]. The mean hourly water production and standard deviation of each site are calculated to assess the production risk [40]. The standard deviation is used to analyse the σ and 2σ confidence intervals, above which 83.7% and 97.5% of water production lies. A higher number indicates more reliable water production over the course of the year.

5 Results and discussion of AWG-technology evaluation and location analysis performance evaluation for different technologies

The energy performance of active AWG technologies is highly dependent on the climatic conditions of the site.First, the three active AWG technologies are compared in terms of their specific energy consumption and water production. The annual performance of the technologies is then analysed using the site analysis model described above, using hourly weather data to evaluate production efficiencies for different geological sites and climates. The calculated specific water costs are used for economic evaluation and comparison with seawater desalination and bottled water. Finally, an analysis of the volatility of water production is carried out to assess the risk of having inconsistent water production over the year.

Table 10 Parameters of AWG technologies for economic analysis

Parameter	CC- AWG	Ads.-Des.- AWG	Abs.-Des.- AWG	Unit	Comment/References
AWG purchase price	50,000	100,000	100,000	[US$]	Table 1; Estimation
Operating life	15	15	15	[years]	Assumed
Annual maintenance cost	3	3	3	[% of purchase price]	[75]
Salvage value	0	0	0	[% of purchase price]	Assumed

5.1 Thermodynamic performance and efficiency evaluation of AWG technologies

5.1.1 Active cooling condensation AWG results

The efficiency of active cooling condensation is highly dependent on the ambient climatic conditions. Figure 11 (left) shows the specific energy consumption for different temperatures and relative humidities. In very hot and humid climatic conditions, the lowest possible specific energy consumption is around 0.17 kWh/kg. The limit of the climate range in which water can be produced depends on the condensation temperature. If it is below freezing point, the AWG machine would freeze, requiring the machine to be heated and significantly reducing its energy efficiency. Figure 11 (right) shows the lowest possible operating points in terms of temperature and relative humidity for the CC AWG model.

5.1.2 Active adsorption–desorption AWG results

In sorptive AWG technologies, the largest energy requirement is for desorption of the water from the desiccant. As the water is extracted from the sorbent by heating the air and the adsorbent bed, the composition of the air plays an inverse role in the energy efficiency of the system compared to CC AWG. Referring to Fig. 12, higher relative humidity levels result in higher specific energy consumption because more total air has to be heated to remove the adsorbed water from the adsorbent bed. Drier and warmer conditions favour the desorption process energetically, resulting in lower specific energy consumption, as less desorption air needs to be heated to reach the desorption temperature of the desiccant. At a low relative humidity of 20% for both materials considered, the SEC increases again at higher daytime temperatures. This is because, assuming the same absolute humidity at night and a temperature decrease of 7 °C compared to the daytime temperature, the absorption potential of the materials is lower, as shown in Fig. 5. Over the climatic range considered, the SECs are significantly higher compared to the other AWG technologies. However, the required desorption temperatures are at a relatively low level, so the required energy can be provided by solar thermal systems, as shown in Fig. 13 for MIL-101(Cr).

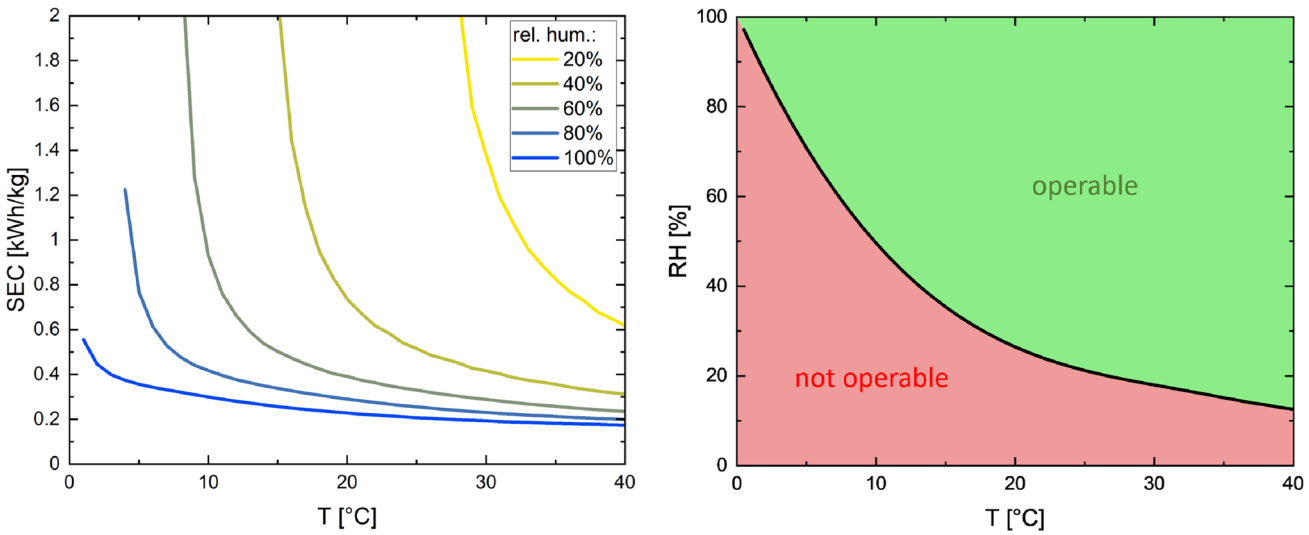

Fig. 11 Left: Specific energy consumption of the CC AWG model calculated for temperature and relative humidity combinations using optimised operating point of electrical energy input and airflow rate. Right: Lowest possible operating points of ambient air temperature and relative humidity for cooling condensation AWG before the condensation temperature reaches freezing point

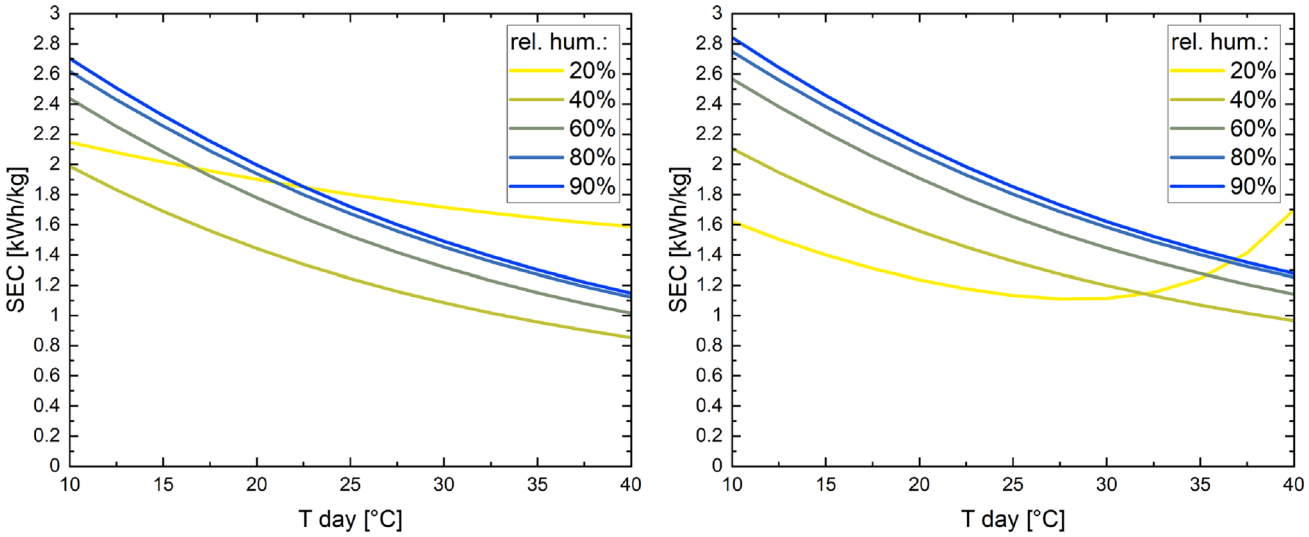

Fig. 12 Specific electrical energy consumption of an adsorption–desorption AWG using MIL-101(Cr) (left) and Co2Cl2BTDD (right) as adsorbent, assuming that the average night temperature is 7 °C colder than the day temperature and that the absolute humidity remains the same during the night and day

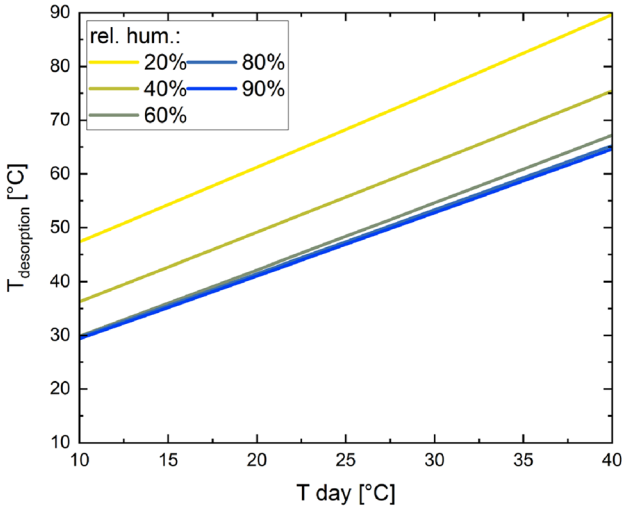

Fig. 13 Desorption temperatures of the adsorption–desorption AWG model calculated for different day temperatures and humidity with a collection fraction of 0.7 using MIL-101(Cr) as adsorbent

5.1.3 Active absorption–desorption AWG results

The specific energy consumption of highly concentrated lithium chloride and potassium acetate aqueous solutions are analysed, as shown in Fig. 14. The use of lithium chloride solution shows a lower specific energy consumption than the use of potassium acetate salt solution with the lowest SEC at about 0.1 kWh/kg (lithium chloride solution) and 0.13 kWh/kg (potassium acetate solution). However, due to the high corrosiveness of lithium chloride, higher quality materials must be used, resulting in higher unit costs. The lower limit of relative humidity is around 40% for both solutions, which is higher compared to other AWGs, but a steeper drop in SEC is calculated with increasing relative humidity due to the higher water uptake potential, see Fig. 5. Lower specific energy requirements are achieved even in drier conditions compared to the CC AWG and the adsorption–desorption AWG. However, the SEC range is higher than that of the CC AWG and the adsorption–desorption AWG.

Similar to the adsorption–desorption process, most of the energy is used to heat the solvent to evaporate the absorbed water out of solution. The required regeneration temperature is calculated to be 135 °C for the lithium chloride solution and 132 °C for the potassium acetate solution. The distribution of energy required for the three active AWG processes under different climatic conditions is shown in Fig. 15. About 90 % of the energy is used to cool the ambient air (CC AWG)

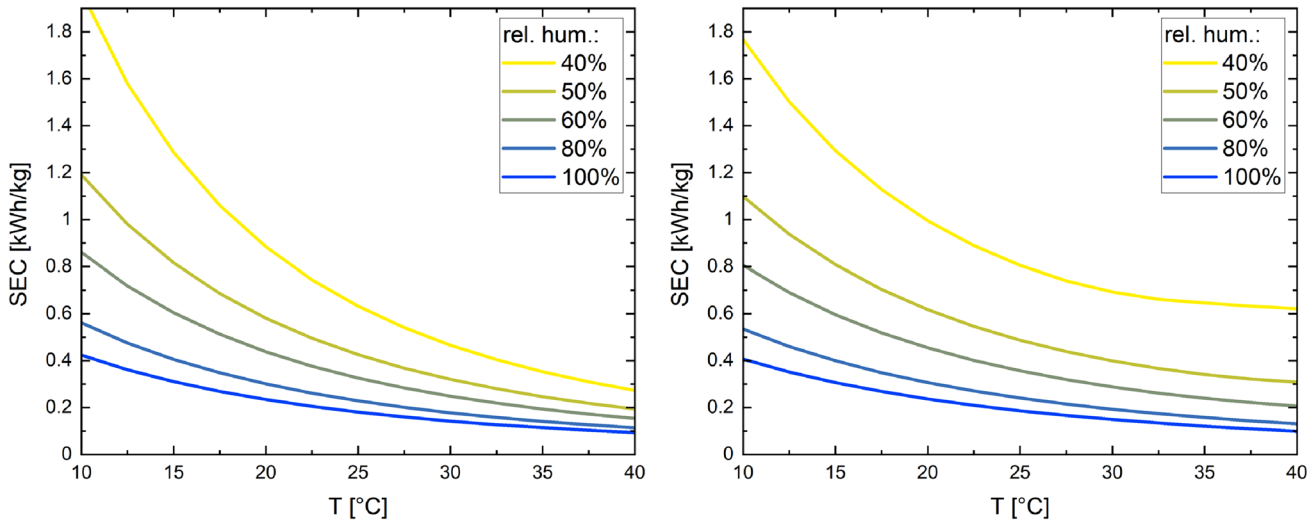

Fig. 14 Specific energy consumption calculated with the absorption–desorption AWG model using lithium chloride (left) and potassium acetate (right) salt solutions using parameters of Table 7 and a resulting regeneration temperature of 134.6 °C

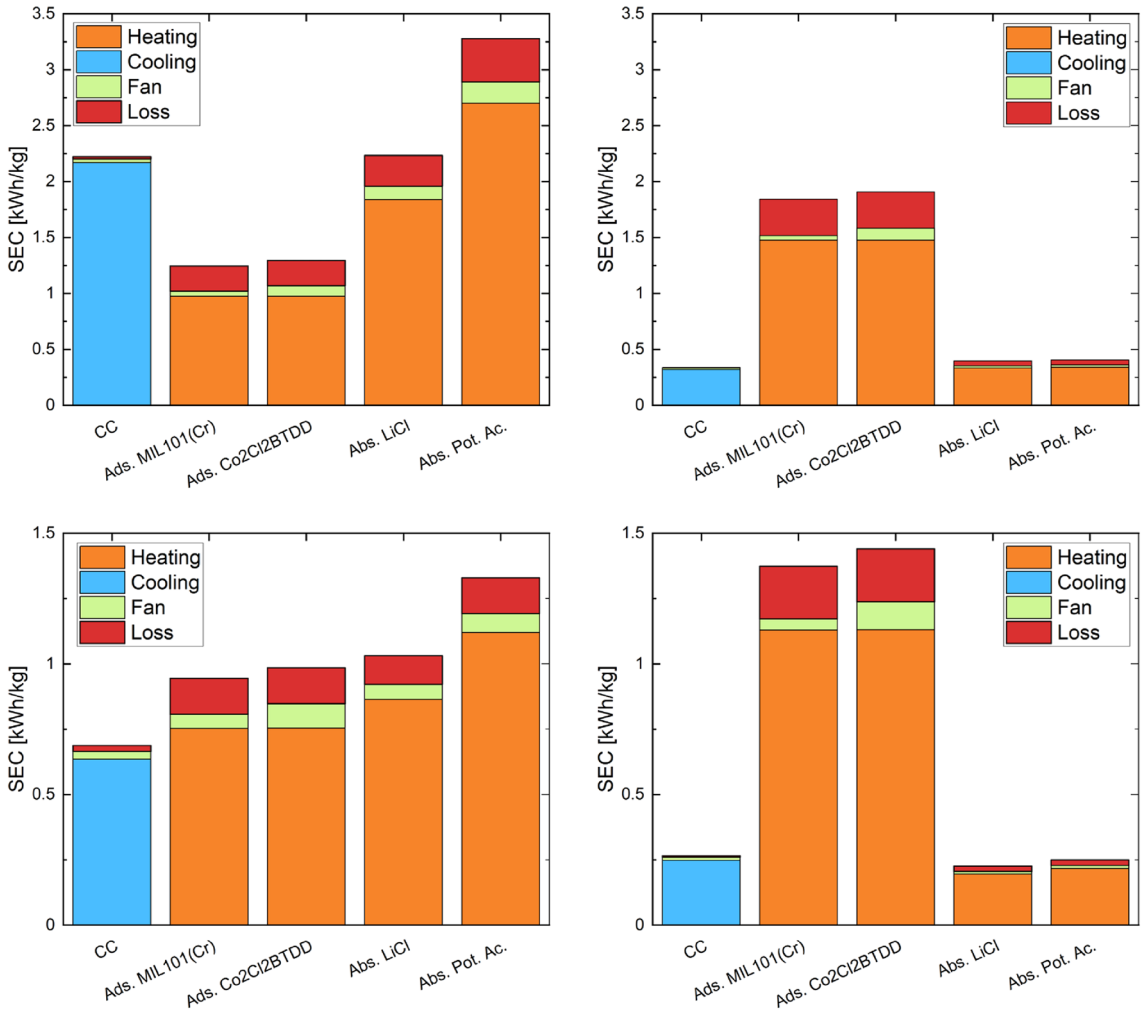

Fig. 15 Distribution of specific energy consumption for the different AWG calculation models at cold and dry (20 °C, 30% RH; top left), cold and humid (20 °C, 70% RH; top right), warm and dry (30 °C, 30% RH; bottom left), warm and humid (30 °C, 70% RH; bottom right)

or about 80% to heat the air and the adsorbent bed or desiccant liquid for desorption of the bound water. The remaining energy is used to generate the required air flow and to account for thermal losses to the environment. Thermal losses are significantly higher for the desiccant based AWGs because the temperature difference with the air is much greater. The energy required for pumps in absorption–desorption AWGs is not included in this graph as it represents less than 1% of the total energy requirement. The results show that different AWG technologies can be energetically advantageous for different climatic conditions. For colder temperatures and high humidity (top right), the absorption–desorption AWG and the CC AWG are most energy efficient. In colder and dry conditions (top left), the adsorption–desorption AWGs have the lowest specific energy demand, while in warmer conditions either the CC AWG (bottom left) or the absorption–desorption AWG (bottom right) are energetically more efficient. This indicates that for realistic, fluctuating climatic conditions between day and night , as well as different seasonal periods, an overall analysis for different locations over a whole year is useful.

5.2 Location performance analysis and economical evaluation of AWG technologies

The analysis of the AWG technologies is carried out using the models previously described for the selected global sites over a full year period to compare the energy efficiency of the systems and to assess the resulting water costs in relation to water production via desalination and transport and bottled water. Water production over the year is analysed and discussed in terms of production risks for a stable water supply.

5.2.1 Truck and pipeline water transport

The specific costs of water production and transport depend linearly on the fuel price at the location and the distance to the destination of water use, as shown in Fig. 16. For each site analysed, the specific cost of water is calculated using the parameters from Table 9. The water production cost is a small percentage of the total cost compared to the transport cost. For short distances, the production cost is about 20% (1.53 US$/m^3 for an annual water production of 50,000 m^3) of the total cost, which share decreases significantly with increasing distance.

5.2.2 Specific energy consumption analysis

Comparing the SECs for the AWG technologies in the location analysis, it can be seen that the adsorption–desorption AWG also has the highest specific energy demand for all sites, as shown in Fig. 17. The specific energy demand of the CC AWG is in the same order of magnitude as that of the absorption–desorption AWG. The specific energy demand of the CC AWG model is on average about 30% higher than that of the absorption–desorption AWG model with 0.422 kWh/kg compared to 0.386 kWh/kg. The strongest influencing parameter for the specific energy demand of both CC AWG and absorption–desorption AWG is the absolute humidity for which a clear tendency of an increasing specific energy demand with decreasing absolute humidity can be observed. This tendency is not so clear for the absorption–desorption AWGs, as a lot of water can be absorbed into the liquid phase at particularly high peak

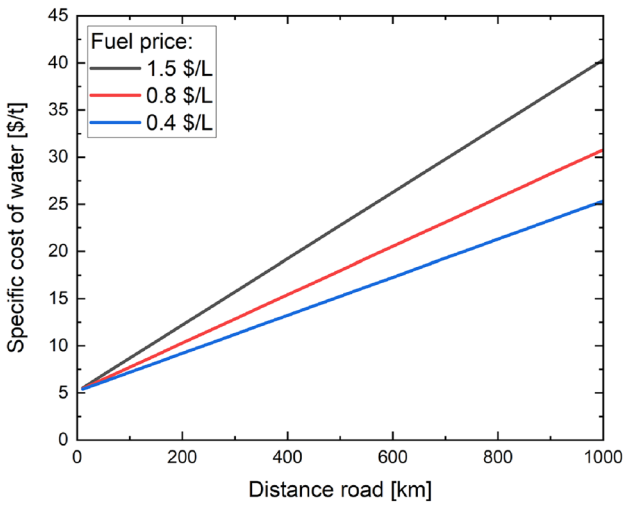

Fig. 16 Specific cost of water, including production and transport by truck, as a function of the distance from the nearest shore to the point of use, for different fuel prices and a water production of 50,000 m^3/year

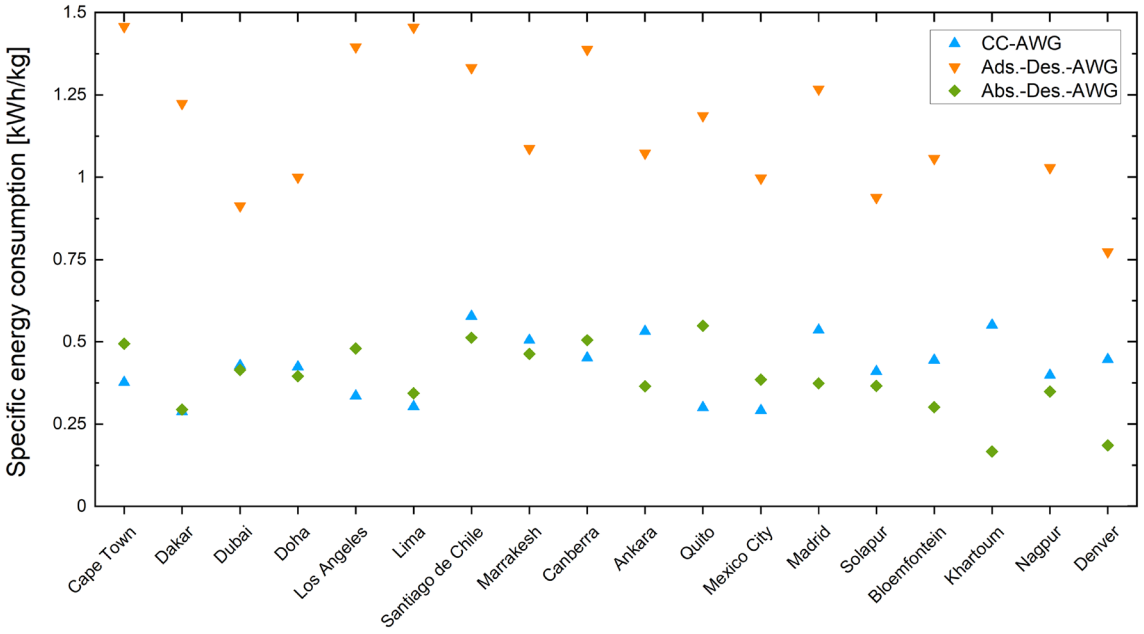

Fig. 17 Specific electricity consumption for water production with different AWG technologies for each site analysed, sorted by the shortest distance to shore from left to right for an annual production of 50,000 m^3 of water

humidity (see Fig. 5), and thus a short-term high absolute humidity greatly increases water production and efficiency. This effect also applies to the comparison with the adsorption–desorption AWG. With an average SEC of 1.156 kWh/kg across all sites, the adsorption–desorption AWG significantly higher in terms of energy demand than the other AWGs. However, the required desorption temperature level is relatively low and a day-night cycle is applied, so that meeting the energy demand with solar thermal energy is a reasonable alternative to drawing electricity from the grid. This would result in a fully off-grid solution, as proposed by most research, for example Kim et al [52].

5.2.3 Specific water cost analysis

The results of the cost calculation for each location are shown in Fig. 18, including the costs of bottled water and water production by desalination and transport. The specific cost of water increases with distance from the coast. Local fuel costs have a direct impact on transport costs. For coastal sites, only RO production costs are considered, resulting in a low specific water production cost of about 1.50 US$/t. Even in locations with very low electricity costs (e.g. Dubai, Doha), which proportionally influence the specific water production costs for AWG systems, this threshold is not reached, but is at least one order of magnitude higher. For longer water transport distances, the energy costs of AWG technologies are closer to the water costs. For Bloemfontein and other locations with distances to the coast greater than 600 km, the water production costs of absorption–desorption AWG and CC AWG are about the same as the specific water costs of truck transport. For Khartoum, absorption–desorption AWG and CC AWG are cheaper than water transport due to very low energy costs and favourable climatic conditions for atmospheric water production. On average for the locations analysed, the absorption–desorption AWG has the lowest operating cost at 61.88 US$/t, followed by the CC AWG at 89.32 US$/t and the adsorption–desorption AWG at 306.16 US$/t. Compared to bottled water with an average of 581.11 US$/t , all three AWG technologies analysed are advantageous in terms of cost.

The ratio of energy costs to total water costs is shown in Table 11. As expected, the results show that in locations with higher water production and lower energy costs, the energy costs far exceed the investment costs, e.g. in Dakar, where energy costs represent 92% (CC), 95% (absorption–desorption) and 63% (adsorption–desorption) of the total costs. On average over all sites, energy costs are the driving cost factors for CC AWG and absorption–desorption AWG at 68% and 82% respectively, while energy and investment costs are equal on average for adsorption–desorption AWG. These results, together with the cost analysis of the sites, make it clear that the primary focus for optimisation must be on increasing energy efficiency or implementing alternative energy supply concepts such as renewable energy. Although reducing production costs is also a viable option, it represents only a small part of the total water production costs.

Table 11 Energy cost to total water cost ratio for each AWG technology and the analyzed locations

City	$Eval^{CC}_{elec/total}$	$Eval^{Ads.-Des.}_{elec/total}$	$Eval^{Abs.-Des.}_{elec/total}$
Bloemfontein	0.42	0.38	0.63
Cape Town	0.65	0.46	0.87
Khartoum	0.57	0.13	0.32
Dakar	0.92	0.63	0.95
Marrakesh	0.74	0.48	0.86
Solapur	0.89	0.45	0.91
Nagpur	0.88	0.46	0.91
Dubai	0.87	0.44	0.91
Doha	0.68	0.2	0.77
Ankara	0.63	0.59	0.84
Canberra	0.77	0.76	0.95
Madrid	0.74	0.64	0.86
Los Angeles	0.79	0.63	0.93
Denver	0.42	0.4	0.54
Mexico City	0.38	0.63	0.89
Santiago	0.52	0.58	0.88
Quito	0.4	0.45	0.88
Lima	0.91	0.69	0.95
Total average	0.68	0.5	0.82

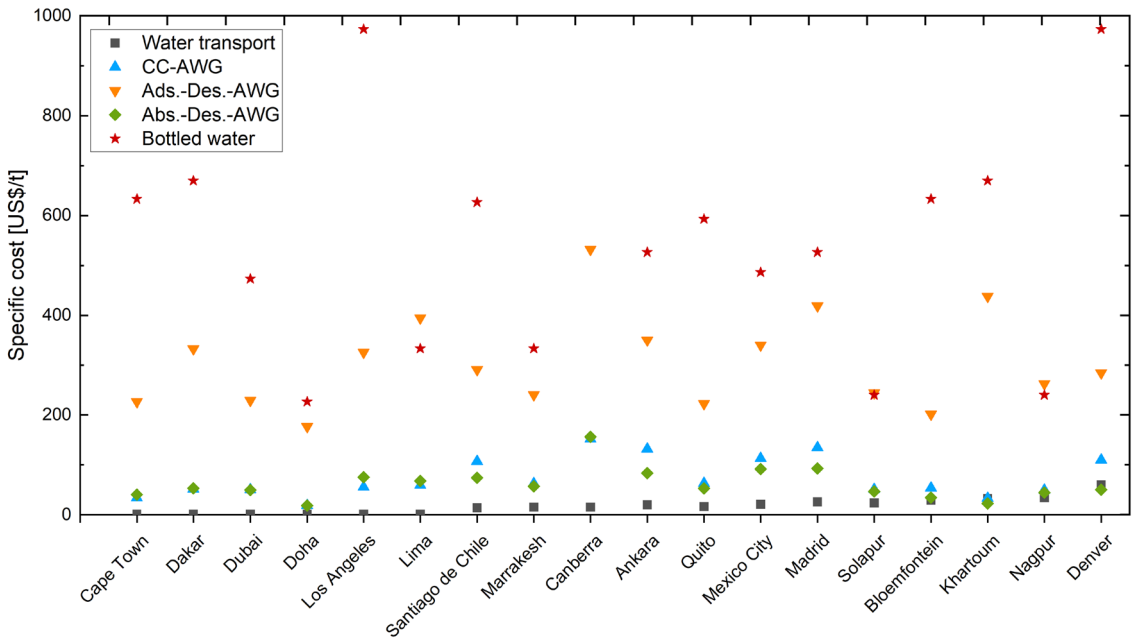

Fig. 18 Specific costs for water production with different AWG technologies for each site analysed, sorted by the lowest distance to shore from left to right compared to total water production with truck transport costs for an annual production of 50,000 m^3 of water and local bottled water prices

5.2.4 Water production and availability risk analysis

Mean water production and confidence intervals of production are shown in Tables 12, 13, 14 for each technology. Using these confidence intervals, we can analyse how much water production varies over the year. As the volatility increases, so does the risk of having no water production for an extended period of time. For the CC AWG and the absorption–desorption AWG, large standard deviations were found for most sites, which implies a high risk of inconsistent water production

Table 12 Mean water production μ in [L/h], standard deviation σ and confidence intervals ($\mu - \sigma$, $\mu - 2\sigma$) of CC AWG for each analysed location

City	μ	σ	$\mu - \sigma$	$\mu - 2\sigma$
Bloemfontein	17.74	48.25	0	0
Cape Town	54.19	72.95	0	0
Khartoum	42.45	58.14	0	0
Dakar	184.39	41.06	143.33	102.27
Marrakesh	41.68	59.14	0	0
Solapur	129.31	65.83	63.48	0
Nagpur	123.56	78.33	45.23	0
Dubai	116.02	54.5	61.52	7.02
Doha	110.35	63.66	46.69	0
Ankara	13.13	38.42	0	0
Canberra	19.6	49.85	0	0
Madrid	19.14	44.92	0	0
Los Angeles	59.5	79.45	0	0
Denver	8.71	34.62	0	0
Mexico City	7.69	36.65	0	0
Santiago	11.63	34.43	0	0
Quito	58.81	75.65	0	0
Lima	139.43	71.75	67.68	0

Negative results are set to zero

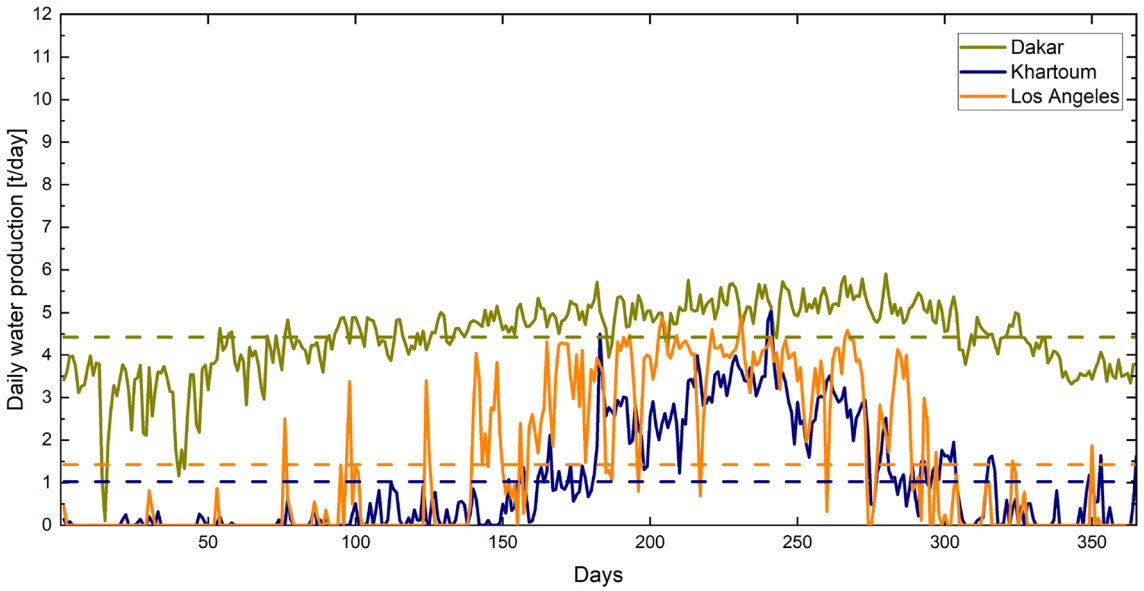

Fig. 19 Daily water production over a year of CC AWG for the locations Dakar, Khartoum and Los Angeles. Average values of water production are shown as dashed lines

throughout the year. The most promising location for constant water production is Dakar with a 2σ value of 102.27 L per hour (CC) or 119.72 L per hour (absorption–desorption), meaning that at least this amount of water can be produced 97.5% of the time. For the σ confidence levels, more locations such as Dubai or Lima can produce more than 60 L per h (CC) or 100 L per h (absorption–desorption) for 83.7% of the days. The large variation in production and the differences between the different locations can also be seen in Figs. 19, 21 and 22, which show the water production over the year for the three AWG technologies for the three distinct locations of Dakar, Khartoum and Los Angeles. In Dakar, where climatic conditions vary less over the year, water production is more stable than in Khartoum or Los Angeles. At these sites, water can be produced mainly during the warm and humid summer months. In contrast, the adsorption–desorption analysis (Fig. 21) shows a much

more constant water production. This is due to the fact that the upper water capacity limit of the adsorbent is constantly reached at most sites and therefore the production is stable throughout the year, as shown by the high σ and 2σ values. Only a few sites, such as Khartoum or Denver, do not achieve this and experience larger fluctuations in water production.

In summary, the high volatility of production must be taken into account when planning the implementation of AWG technologies to ensure a constant water supply. Therefore, AWG technologies work best when used as an additional source of water to complement conventional options. Relying solely on AWG technologies for water supply in these locations is not a viable option.

6 Limitations of study

This chapter discusses the limitations, simplifying assumptions, and potential biases of this study.

Basic economical evaluation: Only a relatively simple economic analysis is considered in this study to provide a baseline analysis. More in-depth analysis of cash flow, financing risks, etc. is not included.

Modell parameters and assumptions: Many model parameters such as the purchase price of adsorption–desorption and absorption–desorption AWGs or operating parameters had to be estimated as no data points are available in the literature. These parameters may change in the future as more research is published or technologies become commercially available.

No exergy efficiency analysis for second law efficiency of AWG technologies: The models developed use only the first law of thermodynamics. Further studies implementing exergy efficiency analysis in the global analysis could prove useful to evaluate the second law efficiency of the AWG systems (e.g., Kim et al. [32] for second law efficiency analysis for adsorption–desorption AWG, Bahman and Groll [76] for second law analysis of air cooling units).

Not considering advanced plant design and control strategies: The efficiency of the technologies could be significantly increased by more complex plant designs, such as multi-stage concepts of adsorption–desorption AWG or different solution management concepts for absorption–desorption AWG [30, 34]. These are current areas of research that will become increasingly important in the future.

Life cycle analysis, environmental impact: A life cycle analysis would be useful to assess the overall impacts, including economic and environmental impacts, of AWG technologies. For example, the impacts and costs of disposal are not considered in this study.

Local regulatory guidelines, subsidies or government legislation: This study did not consider local government subsidies or barriers to the implementation of AWG technologies at the sites analysed.

Focus on bottled water and desalination for price comparisons; neglect of comparison with tap water: An economic comparison with tap water was not made because tap water is often locally subsidised and varies widely in quality, making it less comparable between sites.

7 Conclusion and outlook on future research

Water scarcity is one of the global challenges facing politics, business and science in the twenty-first century, threatening the livelihoods and quality of life of millions of people. Climate change will make water scarcity an even greater global systemic challenge in the future. Harnessing atmospheric moisture can make an important contribution to solving this challenge. In addition to water supply in water scarce areas, the use of decentralised and possibly self-sufficient water supply is an important requirement in the future scenarios of many technological fields. The scientific literature on the evaluation of the economic performance of AWGs, especially for desiccant-based AWGs, is limited. While existing scientific research mainly deals with technical aspects, there is no global analysis that evaluates the performance of AWGs taking into account seasonal and intra-day variations in climatic conditions. Therefore, this paper takes a first step towards comparing different active AWG technologies by implementing a framework for analysing the energetic and economic efficiency on a global scale.

Our results show that active AWG systems could be used as an alternative to water production and truck transport, as long as the location of water use is far from coasts or other water-rich regions. Compared to the price of bottled water, it is economically advantageous in all locations analysed. Absorptive systems were shown to have an energy efficiency advantage over conventional cooling condensation systems, but require a higher level of technology and process and plant design development. Adsorption-desorption AWGs are best suited for off-grid operation with solar power due to low desorption temperature requirements and convenient use of the day-night cycle. Overall, the cost of energy is still

significantly higher than the cost of desalinating and transporting seawater to most locations around the world. This shows that AWG technologies are only economically competitive in the premium water market, e.g. bottled water. The analysis of the ratio of energy cost to total cost of water produced by the AWG technologies showed that most of the cost is produced by energy consumption (CC AWG: 68%, absorption–desorption AWG: 82%, adsorption–desorption AWG: 50%). This indicates that improving energy efficiency would significantly reduce the cost of water production.

A risk analysis of water production showed that at most of the sites analysed, there is a significant variation in water production over the course of a year for all of the AWG technologies. Relying solely on AWG technologies for water supply at these sites is not a viable option.

The current study can be extended by future research that could further investigate the overall environmental impact of AWG technologies using life cycle analysis to assess the carbon footprint. Investigations into local regulatory guidelines, subsidies or policies that could prove to be supportive or hindering to the implementation would also be beneficial to the realisation of future AWG technology projects.

Author contributions JP and AD conceived of the presented idea. JP designed the model and the computational framework and analysed the data. JP performed the calculations and wrote the manuscript with reviews from all authors. All authors provided critical feedback and helped shape the research, analysis and manuscript.

Funding Open Access funding enabled and organized by Projekt DEAL.

Data availability Data publicly available: Global electricity and fuel prices for the analysed locations are available at: https://www.globalpetrolprices.com/ [72]. Bottled water prices for the analysed locations are available at: https://www.globalproductprices.com/ [74]. Hourly temperature, relative humidity and air pressure data are generated using Meteonorm 8.0 [71]. Data available with the paper or supplementary information: The authors declare that the data supporting the findings of this study are available within the paper.

Declarations

Competing interests The authors declare no competing interests.

Appendix A: Water uptake graph adsorption–desorption

See Fig. 20.

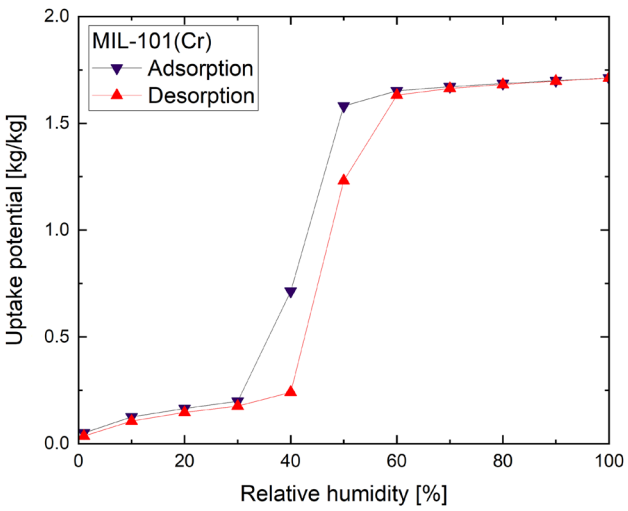

Fig. 20 Water uptake potential for full adsorption and desorption cycle for MIL-101(Cr) at a adsorption temperature of 15 °C and a desorption temperature of 70 °C using adsorbent material data from Gordeeva et al. [61]

Appendix B: Water production tables and graphs

See Figs. 21, 22 and Tables 13, 14.

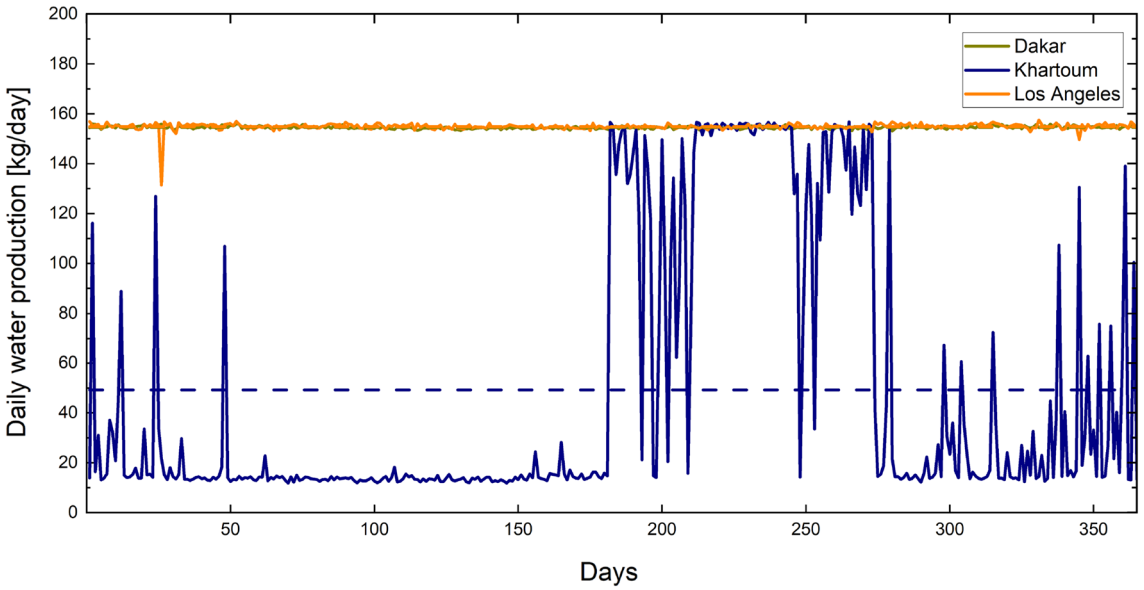

Fig. 21 Daily water production over a year of adsorption–desorption AWG for the locations Dakar, Khartoum and Los Angeles. Average values of water production are shown as dashed lines

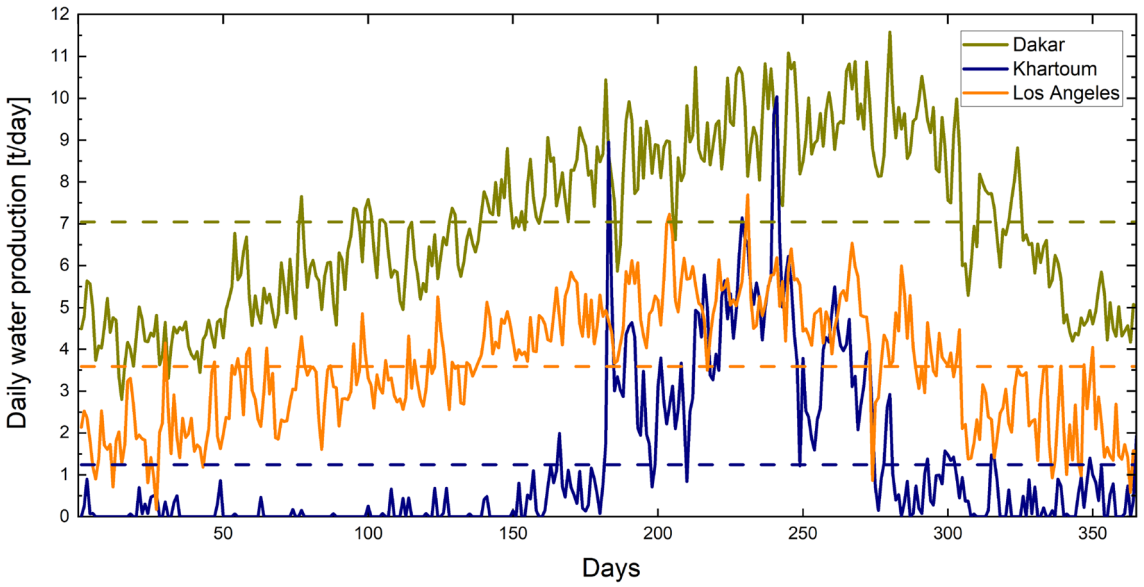

Fig. 22 Daily water production over a year of absorption–desorption AWG for the locations Dakar, Khartoum and Los Angeles. Average values of water production are shown as dashed lines

Table 13 Mean water production μ in [L/h], standard deviation σ and confidence intervals ($\mu - \sigma$, $\mu - 2\sigma$) of Ads.-Des.-AWG for each analysed location

City	μ	σ	$\mu - \sigma$	$\mu - 2\sigma$
Bloemfontein	6.27	1.06	5.21	4.15
Cape Town	6.47	0.04	6.43	6.4
Khartoum	2.05	2.3	0	0
Dakar	6.44	0.02	6.42	6.39
Marrakesh	6.27	0.755	5.51	4.76
Solapur	5.85	1.46	4.39	2.93
Nagpur	5.54	1.91	3.63	1.72
Dubai	6.11	1	5.11	4.11
Doha	5.58	1.78	3.8	2.01
Ankara	5.45	2.23	3.22	0.99
Canberra	6.26	1.21	5.06	3.85
Madrid	5.28	1.98	3.3	1.32
Los Angeles	6.45	0.06	6.39	6.33
Denver	4.59	2.87	1.72	0
Mexico City	6.17	0.91	5.26	4.34
Santiago	6.46	0.48	5.98	5.49
Quito	6.45	0.04	6.42	6.38
Lima	6.42	0.02	6.4	6.37

Negative results are set to zero

Table 14 Mean water production μ in [L/h], standard deviation σ and confidence intervals ($\mu - \sigma$, $\mu - 2\sigma$) of Abs.-Des.-AWG for each analysed location

City	μ	σ	$\mu - \sigma$	$\mu - 2\sigma$
Bloemfontein	60.98	72.99	0	0
Cape Town	156.78	44.46	112.32	67.87
Khartoum	51.71	88.67	0	0
Dakar	293.36	86.82	206.54	119.72
Marrakesh	95.78	66.88	28.9	0
Solapur	189.86	117.29	72.57	0
Nagpur	204.16	137.02	67.14	0
Dubai	186.1	83.86	102.25	18.39
Doha	184.46	99.38	85.08	0
Ankara	57.13	60.89	0	0
Canberra	95.52	66.47	29.05	0
Madrid	58.83	64.36	0	0
Los Angeles	149.44	66.4	83.04	16.65
Denver	33.88	59.34	0	0
Mexico City	80.17	72.41	7.76	0
Santiago	89.1	55.28	33.82	0
Quito	125.53	41.04	84.49	43.44
Lima	231.17	43.49	187.67	144.18

Negative results are set to zero

References

1. WHO. Drinking-water report. 2022. https://www.who.int/news-room/fact-sheets/detail/drinking-water.
2. Elimelech M. The global challenge for adequate and safe water. J Water Supply: Res Technol - Aqua. 2006;55(1):3–10. https://doi.org/10.2166/aqua.2005.064.
3. Tu Y, Wang R, Zhang Y, Wang J. Progress and expectation of atmospheric water harvesting. Joule. 2018;2(8):1452–75. https://doi.org/10.1016/j.joule.2018.07.015.

4. Mekonnen MM, Hoekstra AY. Four billion people facing severe water scarcity. Sci Adv. 2016;2(2): e1500323. https://doi.org/10.1126/sciadv.1500323.
5. Koronkevich NI, Barabanova EA, Zaitseva IS. Assessment of modern water consumption in the world and on continents and its impact on the annual river runoff. Her Russ Acad Sci. 2022;92(2):199–206. https://doi.org/10.1134/S1019331622020034.
6. Ali Y. Carbon, water and land use accounting: consumption vs production perspectives. Renew Sustain Energy Rev. 2017;67:921–34. https://doi.org/10.1016/j.rser.2016.09.022.
7. Scanlon BR, et al. Global synthesis of groundwater recharge in semiarid and arid regions. Hydrol Process. 2006;20(15):3335–70. https://doi.org/10.1002/hyp.6335.
8. Valois R, MacDonell S, Núñez Cobo JH, Maureira-Cortés H. Groundwater level trends and recharge event characterization using historical observed data in semi-arid Chile. Hydrol Sci J. 2020;65(4):597–609. https://doi.org/10.1080/02626667.2020.1711912.
9. Alfarrah N, Walraevens K. Groundwater overexploitation and seawater intrusion in coastal areas of arid and semi-arid regions. Water. 2018;10(2):143. https://doi.org/10.3390/w10020143.
10. Cirilo JA. Public water resources policy for the semi-arid region. EstudosAvançados. 2009. https://api.semanticscholar.org/CorpusID:55101895.
11. Lamei A, van der Zaag P, von Münch E. Basic cost equations to estimate unit production costs for RO desalination and long-distance piping to supply water to tourism-dominated arid coastal regions of Egypt. Desalination. 2008;225(1–3):1–12. https://doi.org/10.1016/j.desal.2007.08.003.
12. Parag Y, Elimelech E, Opher T. Bottled water: an evidence-based overview of economic viability, environmental impact, and social equity. Sustainability. 2023;15(12):9760. https://doi.org/10.3390/su15129760.
13. Ai Z, Ishihama F, Hanasaki N. Mapping current and future seawater desalination plants globally using species distribution models. Water Resour Res. 2022. https://doi.org/10.1029/2021WR031156.
14. Shahzad MW, Burhan M, Ang L, Ng KC. Energy-water-environment nexus underpinning future desalination sustainability. Desalination. 2017;413:52–64. https://doi.org/10.1016/j.desal.2017.03.009.
15. Elimelech M, Phillip WA. The future of seawater desalination: energy, technology, and the environment. Science (New York, NY). 2011;333(6043):712–7. https://doi.org/10.1126/science.1200488.
16. Cornejo PK, Santana MVE, Hokanson DR, Mihelcic JR, Zhang Q. Carbon footprint of water reuse and desalination: a review of greenhouse gas emissions and estimation tools. J Water Reuse Desalin. 2014;4(4):238–52. https://doi.org/10.2166/wrd.2014.058.
17. Liu J, Chen S, Wang H, Chen X. Calculation of carbon footprints for water diversion and desalination projects. Energy Procedia. 2015;75:2483–94. https://doi.org/10.1016/j.egypro.2015.07.239.
18. Al-Karaghouli A, Kazmerski LL. Energy consumption and water production cost of conventional and renewable-energy-powered desalination processes. Renew Sustain Energy Rev. 2013;24:343–56. https://doi.org/10.1016/j.rser.2012.12.064.
19. Caldera U, Bogdanov D, Breyer C. Local cost of seawater RO desalination based on solar PV and wind energy: a global estimate. Desalination. 2016;385:207–16. https://doi.org/10.1016/j.desal.2016.02.004.
20. Ghaffour N, Missimer TM, Amy GL. Technical review and evaluation of the economics of water desalination: current and future challenges for better water supply sustainability. Desalination. 2013;309:197–207. https://doi.org/10.1016/j.desal.2012.10.015.
21. Chang J-S. Understanding the role of ecological indicator use in assessing the effects of desalination plants. Desalination. 2015;365:416–33. https://doi.org/10.1016/j.desal.2015.03.013.
22. Zhou J, Chang VW-C, Fane AG. An improved life cycle impact assessment (LCIA) approach for assessing aquatic eco-toxic impact of brine disposal from seawater desalination plants. Desalination. 2013;308:233–41. https://doi.org/10.1016/j.desal.2012.07.039.
23. Roberts DA, Johnston EL, Knott NA. Impacts of desalination plant discharges on the marine environment: a critical review of published studies. Water Res. 2010;44(18):5117–28. https://doi.org/10.1016/j.watres.2010.04.036.
24. Zhang M, Liu R, Li Y. Diversifying water sources with atmospheric water harvesting to enhance water supply resilience. Sustainability. 2022;14(13):7783. https://doi.org/10.3390/su14137783.
25. Fosso-Kankeu E, Al Alili A, Mittal H, Mamba B. Atmospheric water harvesting development and challenges, vol. 122. Cham: Springer; 2023.
26. Peeters R, Vanderschaeghe H, Rongé J, Martens JA. Energy performance and climate dependency of technologies for fresh water production from atmospheric water vapour. Environ Sci: Water Res Technol. 2020;6(8):2016–34. https://doi.org/10.1039/d0ew00128g.
27. Gido B, Friedler E, Broday DM. Assessment of atmospheric moisture harvesting by direct cooling. Atmos Res. 2016;182:156–62. https://doi.org/10.1016/j.atmosres.2016.07.029.
28. Xu W, Yaghi OM. Metal-organic frameworks for water harvesting from air, anywhere, anytime. ACS Cent Sci. 2020;6(8):1348–54. https://doi.org/10.1021/acscentsci.0c00678.
29. Wang JY, Liu JY, Wang RZ, Wang LW. Experimental investigation on two solar-driven sorption based devices to extract fresh water from atmosphere. Appl Therm Eng. 2017;127:1608–16. https://doi.org/10.1016/j.applthermaleng.2017.09.063.
30. LaPotin A, et al. Dual-stage atmospheric water harvesting device for scalable solar-driven water production. Joule. 2021;5(1):166–82. https://doi.org/10.1016/j.joule.2020.09.008.
31. LaPotin A, Kim H, Rao SR, Wang EN. Adsorption-based atmospheric water harvesting: impact of material and component properties on system-level performance. Acc Chem Res. 2019;52(6):1588–97. https://doi.org/10.1021/acs.accounts.9b00062.
32. Kim H, Rao SR, LaPotin A, Lee S, Wang EN. Thermodynamic analysis and optimization of adsorption-based atmospheric water harvesting. Int J Heat Mass Transf. 2020;161:120253. https://doi.org/10.1016/j.ijheatmasstransfer.2020.120253.
33. Almasarani A, Ahmad IK, El-Amin MF, Brahimi T. Experimental investigations and modeling of atmospheric water generation using a desiccant material. Energies. 2022;15(18):6834. https://doi.org/10.3390/en15186834.
34. Kölking S. Absorptions- und Desorptionsverhalten hoch konzentrierter Elektrolyte für die Trinkwassergewinnung aus Luftfeuchtigkeit, vol. 67 of Berichte aus Forschung und Entwicklung / Fraunhofer-Institut für Grenzflächen- und Bioverfahrenstechnik, IGB. Fraunhofer Verl., Stuttgart. 2015. http://publica.fraunhofer.de/dokumente/N-367270.html.
35. Wang B, Zhou X, Guo Z, Liu W. Recent advances in atmosphere water harvesting: design principle, materials, devices, and applications. Nano Today. 2021;40:101283. https://doi.org/10.1016/j.nantod.2021.101283.

36. Peeters R, Vanderschaeghe H, Rongé J, Martens JA. Fresh water production from atmospheric air: technology and innovation outlook. iScience. 2021;24(11):103266. https://doi.org/10.1016/j.isci.2021.103266.
37. Asim N, et al. Sorbent-based air water-harvesting systems: progress, limitation, and consideration. Rev Environ Sci Bio/Technol. 2021;20(1):257–79. https://doi.org/10.1007/s11157-020-09558-6.
38. Tu R, Hwang Y. Reviews of atmospheric water harvesting technologies. Energy. 2020;201:117630. https://doi.org/10.1016/j.energy.2020.117630.
39. Lord J, et al. Global potential for harvesting drinking water from air using solar energy. Nature. 2021;598(7882):611–7. https://doi.org/10.1038/s41586-021-03900-w.
40. Moghimi F, Ghoddusi H, Asiabanpour B, Behroozikhah M. Is atmospheric water generation an economically viable solution? Clean Technol Environ Policy. 2021;23(3):1045–62. https://doi.org/10.1007/s10098-020-02015-6.
41. ASHRAE American Society of Heating Refrigerating and Air-Conditioning Engineers. ASHRAE handbook—fundamentals. ASHRAE, Atlanta. 2017.
42. Kaseke KF, Wang L. Fog and dew as potable water resources: maximizing harvesting potential and water quality concerns. GeoHealth. 2018;2(10):327–32. https://doi.org/10.1029/2018GH000171.
43. Alahmer A, Al-Dabbas M, Alsaqoor S, Al-Sarayreh A. Utilizing of solar energy for extracting freshwater from atmospheric air. Appl Solar Energy. 2018;54(2):110–8. https://doi.org/10.3103/S0003701X18020044.
44. Bagheri F. Performance investigation of atmospheric water harvesting systems. Water Resour Ind. 2018;20:23–8. https://doi.org/10.1016/j.wri.2018.08.001.
45. Abdo D, et al. Experimental analysis of a compact atmospheric water generator by refrigerant method; 2022. p. 5–8. https://doi.org/10.1109/ICECTA57148.2022.9990304.
46. Bergmair D, Metz SJ, de Lange HC, van Steenhoven AA. System analysis of membrane facilitated water generation from air humidity. Desalination. 2014;339:26–33. https://doi.org/10.1016/j.desal.2014.02.007.
47. Genaq technologies s.l. 2024. https://genaq.com/solutions/. Accessed 30 Jan 2024.
48. Watergen ltd. 2024. https://www.watergen.com/commercial/gen-l/. Accessed 30 Jan 2024.
49. Aerowater private limited. 2024. https://www.airowater.com/products/. Accessed 30 Jan 2024.
50. Bestway (hangzhou) drinking water equipment co., ltd. 2024. https://aquaosmo.en.alibaba.com/index.html?spm=a2700.shop_cp.88.13. Accessed 30 Jan 2024.
51. Imhotep.industries gmbh. 2024. https://imhotep.industries/. Accessed 30 Jan 2024.
52. Kim H, et al. Adsorption-based atmospheric water harvesting device for arid climates. Nat Commun. 2018;9(1):1191. https://doi.org/10.1038/s41467-018-03162-7.
53. Singh RP, Mishra VK, Das RK. Desiccant materials for air conditioning applications—a review. IOP Conf Ser: Mater Sci Eng. 2018;404:012005. https://doi.org/10.1088/1757-899X/404/1/012005.
54. Salikandi M, et al. Recent trends in liquid desiccant materials and cooling systems: application, performance and regeneration characteristics. J Build Eng. 2021;33:101579. https://doi.org/10.1016/j.jobe.2020.101579.
55. Rafique MM, Gandhidasan P, Bahaidarah HM. Liquid desiccant materials and dehumidifiers—a review. Renew Sustain Energy Rev. 2016;56:179–95. https://doi.org/10.1016/j.rser.2015.11.061.
56. Zegenhagen MT, Ricart C, Meyer T, Kühn R, Ziegler F. Experimental investigation of a liquid desiccant system for air dehumidification working with ionic liquids. Energy Procedia. 2015;70:544–51. https://doi.org/10.1016/j.egypro.2015.02.159.
57. Varela RJ, et al. Experimental performance analysis and simulation of an internally cooled liquid desiccant air conditioning system using a novel ionic liquid. 2020. https://doi.org/10.18462/iir.gl.2020.1189.
58. Yang K, et al. Hollow spherical SiO2 micro-container encapsulation of LiCl for high-performance simultaneous heat reallocation and seawater desalination. J Mater Chem A. 2020;8(4):1887–95. https://doi.org/10.1039/C9TA11721K.
59. Khushnood S, et al. Optimized caged silica synthesis with lithium chloride and calcium chloride impregnation for prospective desalination application. J Porous Mater. 2023. https://doi.org/10.1007/s10934-023-01536-x.
60. Kniss A, Blicker M, Eisele M, Michelberger M, Warnke D. Entwicklung und demonstration einer technologie zur nachhaltigen trinkwassergewinnung aus luftfeuchtigkeit—walu: Abschlussbericht zum foerderprogramm efre umwelttechnik des ministeriums fuer umwelt, klima und energiewirtschaft baden-wuerttemberg. 2014. https://pd.lubw.de/97759.
61. Gordeeva LG, Solovyeva MV, Sapienza A, Aristov YI. Potable water extraction from the atmosphere: potential of MOFs. Renew Energy. 2020;148:72–80. https://doi.org/10.1016/j.renene.2019.12.003.
62. Chaudhari SK, Patil KR. Thermodynamic properties of aqueous solutions of lithium chloride. Phys Chem Liq. 2002;40(3):317–25. https://doi.org/10.1080/0031910021000004883.
63. Kosky P, Balmer R, Keat WD, Wise G. Exploring engineering: an introduction to engineering and design. San Diego: Elsevier Science; 2020.
64. Arpagaus C, Bless F, Uhlmann M, Schiffmann J, Bertsch SS. High temperature heat pumps: market overview, state of the art, research status, refrigerants, and application potentials. Energy. 2018;152:985–1010. https://doi.org/10.1016/j.energy.2018.03.166.
65. Greenlee LF, Lawler DF, Freeman BD, Marrot B, Moulin P. Reverse osmosis desalination: water sources, technology, and today's challenges. Water Res. 2009;43(9):2317–48. https://doi.org/10.1016/j.watres.2009.03.010.
66. Fritzmann C, Löwenberg J, Wintgens T, Melin T. State-of-the-art of reverse osmosis desalination. Desalination. 2007;216(1–3):1–76. https://doi.org/10.1016/j.desal.2006.12.009.
67. Marufuzzaman M, Ekşioğlu SD, Hernandez R. Truck versus pipeline transportation cost analysis of wastewater sludge. Transport Res Part A: Policy Pract. 2015;74:14–30. https://doi.org/10.1016/j.tra.2015.02.001.
68. Berwick M, Farooq MU. Truck costing model for transportation managers. 2003.
69. Pootakham T, Kumar A. A comparison of pipeline versus truck transport of bio-oil. Biores Technol. 2010;101(1):414–21. https://doi.org/10.1016/j.biortech.2009.07.077.
70. Pootakham T, Kumar A. Bio-oil transport by pipeline: a techno-economic assessment. Biores Technol. 2010;101(18):7148–54. https://doi.org/10.1016/j.biortech.2010.03.136.

71. Remund J, Müller S, Schmutz M, Graf P. Meteonorm. 2022.
72. Valev N. Globalpetrolprices.com. 2023. https://www.globalpetrolprices.com/. Accessed 15 Aug 2023.
73. Google (n.d.). Google maps directions for the shortest road distance from the locations to the nearest coast. 2023. https://www.google.com/maps/. Accessed 05 Jan 2023.
74. Valev N. Globalproductprices.com. 2024. https://www.globalproductprices.com/. Accessed 17 Jan 2024.
75. Peddireddy VRR. Estimating maintenance CapEx. Columbia University. 2021.
76. Bahman A, Groll E. Second-law analysis to improve the energy efficiency of environmental control unit. 2016.